Chapter II: Atomic Physics Relevant to Fusion Plasmas

As demonstrated in Ch. I, both the atomic physics and the interactions of plasma with the materials of the PFCs (in particular, the first wall of vacuum chamber and divertor targets) play very important role in virtually all edge plasma phenomena including plasma recycling, energy dissipation, divertor detachment, erosion of the PFCs, plasma contamination with impurities, etc. In this chapter, we will focus on the atomic physics issues relevant to fusion plasmas.

Although atomic physics processes at the edge of magnetic fusion devices have some similarity to those in low-temperature gas discharge plasmas (e.g. see [1], [2], [3]), which have been under intense theoretical studies over hundred years, there are also important differences. First, the fusion plasma consists mostly of hydrogenic species, having some (~10%) helium as well as a potentially controlled (deliberately injected), relatively small percentage (~1%) of impurity species for plasma cooling (e.g. neon, argon, etc.), and some fraction of impurities originated from the erosion of the PFC materials (e.g. lithium, beryllium, tungsten, etc.). Secondly, unlike most of the gas discharges that feature rather homogeneous, low temperature (~1 eV) plasmas, the edge plasma parameters in fusion devices are very non-uniform (e.g. the edge plasma temperature in discharge can vary from sub-eV to few hundred eV). As a result, atomic processes taking place in edge plasma are very diverse and ranging from plasma recombination in low-temperature regions to both neutral hydrogen and impurity ionization at high temperatures (we notice that at temperature ~ keV neon can be completely stripped off of all electrons). As we will see, both diversity and inhomogeneity of the edge plasma parameters increase the number of atomic processes that should be allowed for, which complicates the edge plasma description.

In this section, we review basic quantum mechanical features of atomic species relevant for edge plasma studies and discuss the physics behind the Collisional-Radiative Model (CRM) widely used in fusion research for the description of the rate of different atomic processes. We will also consider some important examples of the application of the CRM to atoms, molecules and ions for edge plasma conditions, as well as line radiation transport in edge plasma and its implication for relevant atomic processes.

II.1 Basic quantum mechanical features of atoms, molecules, and ions relevant for magnetic fusion research

As known from quantum mechanics (e.g. see [4]), atoms, molecules and their ions can only occupy some particular quantum energy states bounded between the so-called ground state and ionization (or dissociation) continuum of the corresponding neutral/ion (or the molecule/molecular ion), which represents a free electron and the remaining ion (or separated neutrals and ions). Such states can be related to different electronic configurations and also, in case of molecules, to different rotational and vibrational states. It appears that the neutrals and ions occupying excited states (situated in energy space above the ground state) play important roles in virtually all atomic physics-related processes in edge plasmas even though the relative fraction of such particles is often small. The situation with excited particles is somewhat similar to that of free chemical radicals, which have low concentrations but are important in many chemical reactions (e.g. see [5], [6]).

In this sub-section, we just review the main features of quantum states in the atoms, molecules, and ions relevant for edge plasma (for more details one can refer to [4] and special literature).

We start with quantum states in a hydrogen-like ion having one bound electron and the charge number of nucleus Z (the case Z=1 corresponds to the hydrogen atom). Omitting all relativistic effects, we find [4] that the energy levels, E_n, depend only on the principal quantum number n ($1 \le n < \infty$) and

$$E_n^{H_Z} = -\frac{m_e Z^2 e^4}{2\hbar^2}\frac{1}{n^2}, \qquad \text{(II.1)}$$

where zero energy corresponds to the free electron (continuum), m_e and e are the electron mass and charge, and $\hbar$ is the reduced Planck constant (we neglect here the terms of the order of the ratio of m_e to the nucleon mass M_{nucl}). From Eq. (II.1) it follows that the ionization potential of this hydrogen-like ion from the ground state $n = 1$ is $I_{H_Z} = m_e Z^2 e^4 / 2\hbar^2$. However, it appears that the quantum states with $n > 1$ are not stable and decay rather quickly into states having lower principal quantum numbers. The decay time from the level n to level k ($k < n$) is determined by the Einstein coefficients, $A_{n\to k}^{H_Z}$, which in a quasi-classical Kramers approximation can be written as [3]:

$$A_{n\to k}^{H_Z} \approx \frac{1.6\times 10^{10} Z^4}{n^3 k(n^2 - k^2)} s^{-1}. \qquad \text{(II.2)}$$

For a hydrogen atom, the inverse decay time from the first excited state to the ground one is $A_{2\to 1}^{H} \approx 6\times 10^8 s^{-1}$. In some cases, it is important to have an estimate of the decay time from the level n to all lower levels, which is given by $A_n^{H_Z} = \sum_{k=1}^{k=n-1} A_{n\to k}$. Then from Eq. (II.2) we have

$$A_n^{H_Z} \approx 1.6\times 10^{10}\frac{Z^4}{n^5}\ell n\left(\frac{n^3 - n}{2}\right) s^{-1}. \qquad \text{(II.3)}$$

For a single hydrogen atom in vacuum, the number of available quantum states (the so-called Rydberg states) is not limited. However, in the magnetic fusion environment, this is not the case. Even intuitively it is difficult to imagine hydrogen atom with an effective radius of the electron orbit larger than the average inter-ion distance $\sim n_e^{-1/3}$ (e.g. the Inglis–Teller equation predicts that the highest observable hydrogen quantum state $n_{max} \sim n_e^{-2/15}$ [7]). In practice, isolated high Rydberg states, being affected by the plasma-induced micro-electric field, $E_{micro} \sim e n_e^{2/3}$, eventually disappear and merge with continuum, so that the number of states in Eq. (II.3) becomes finite. One can see this from the intensities of the Balmer series of hydrogen lines obtained from a wall-stabilized arc discharge and recombining divertor plasma of Alcator C-Mod tokamak (Fig. II.1). In the arc plasma with density $n_e \approx 10^{17} cm^{-3}$, the highest distinguishable Rydberg state corresponds to $n \approx 7$ (Fig. II.1a), whereas in the divertor plasma of Alcator C-Mod, having a somewhat lower density, $n_e \approx 10^{15} cm^{-3}$, the Balmer lines merge to continuum at $n \approx 11$ (Fig. II.1b).

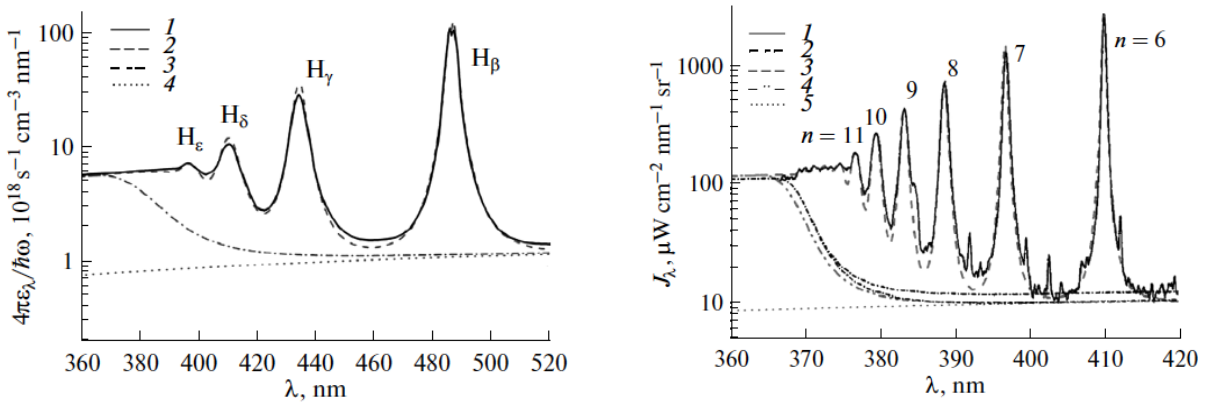

(a) (b)

Fig. II.1. The Balmer series of lines (solid curves) obtained from a wall-stabilized arc discharge (a, Reproduced with permission from [8], © Springer 2016) and recombining divertor plasma of Alcator C-Mod tokamak (b, Reproduced with permission from [48], © AIP Publishing 1998).

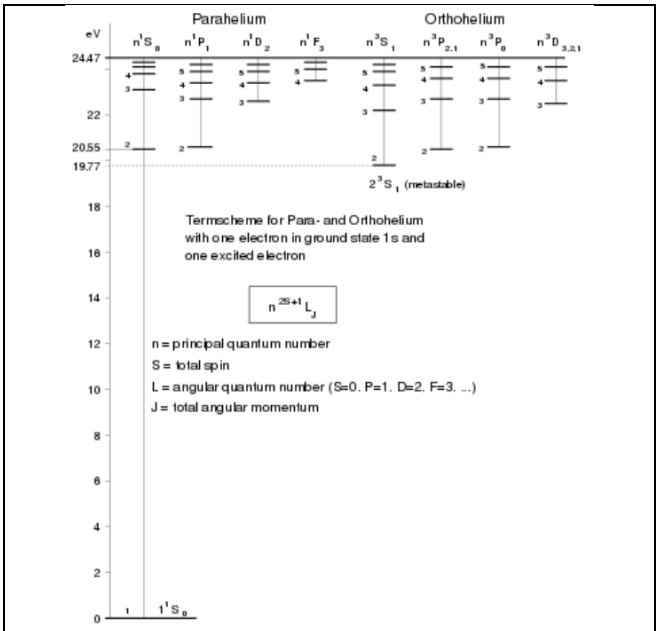

Fig. II.2. The energy levels in the helium atom, singlets (para-) and triplets (ortho-), for the case with one electron on the ground state (1s) and one excited electron (taken from Wikipedia, https://en.wikipedia.org/wiki/Helium_atom)

In magnetic fusion devices having strong magnetic field, an additional reason limiting available number of Rydberg states can be related to the Zeeman splitting of excited states and their spontaneous ionization by the effective electric field, $E_B \sim (V_N / c)B$, caused by neutral motion across the magnetic field (here B is the magnetic field strength, c is the speed of light, and V_N is the speed of the neutral).

As we see, the structure of the quantum states in a hydrogen-like ion/hydrogen atom is rather simple. This "simplicity" is due to the peculiar degeneracy of quantum states over electron orbital angular momentum. However, the situation quickly becomes much more complex for atoms/ions having few electrons. As an example, in Fig. II.2 one can see the helium quantum energy levels, which now depend also on the total orbital angular momentum, L=0, 1, 2, … (which is usually denoted by the letters S, P, …), spin, **S**, and total angular momentum **J**=**L**+**S** (see the insert in Fig. II.2). The only exception is negative hydrogen ion, H^-, also having two electrons, but only one bounded state with a low "ionization" potential of ~0.75 eV. H^- makes (as we will see later) some contribution to divertor plasma recombination but plays an important role in the generation of MeV range neutral beams suitable for plasma heating in magnetic fusion reactors (e.g. see [9] and the references therein).

We notice that some excited quantum states of complex atoms/ions, the so-called "metastable" states (spontaneous transitions from these states to lower energy states are "forbidden" by selection rules [4]), exhibit no spontaneous decay to lower states for a time much longer than $\sim 2\times 10^{-9}\,\mathrm{s}$, which follows from Eq. (II.2) for the transition from the first excited to the ground state in the hydrogen atom. The examples of such metastable states in helium are the triplet electron configuration 2^3S_1 (see Fig. II.2), having extremely long natural life-time ~10^4 s [10], and the singlet state 2^1S_0 which has much shorter, ~20 ms [11], natural life-time. Such long-living metastable states (e.g. 2^3S_1 in helium) play very important role in ionization balance of low temperature, weakly ionized plasma, by providing the so-called Penning ionization channel, $A_* + B \rightarrow A + B^+ + e$, where A_* is a particle on a metastable state with the energy higher than the ionization potential of the particle B (e.g. see [12], [13], [14] and the references therein).

So far, we were discussing quantum effects related to atoms/ions. However, plasma recycling on the PFCs results partly in the formation of molecules, which play an important and somewhat peculiar role in edge plasma processes.

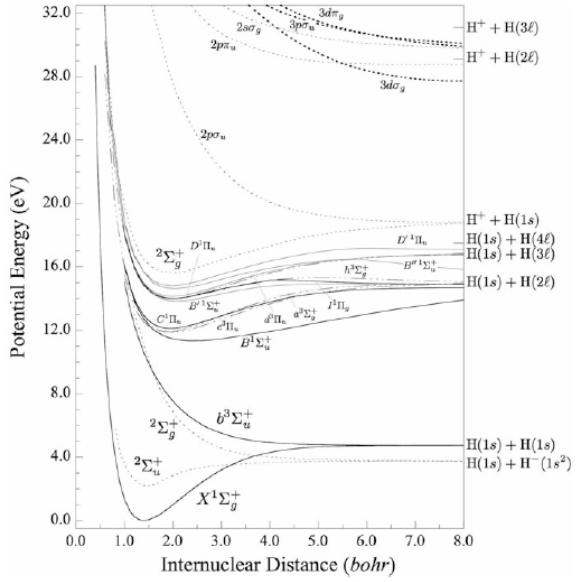

Fig. II.3 Molecular hydrogen terms. Reproduced with permission from [16], © Springer 2012.

Since hydrogen is the major component in fusion plasmas, we will consider mainly the hydrogen molecules. As before, we will distinguish molecules containing different isotopologues of hydrogen molecule (e.g. H_2, D_2, DT, etc.) only when it becomes important, otherwise, we will call them just hydrogen molecules and use the notation H_2. Molecular hydrogen having two nuclei introduces new features in the energy spectrum of the quantum states. Using disparity in electron and nuclei dynamics, related to the difference in their masses, one could start with the analysis of electronic states assuming that the separation distance, R, between the two nuclei is fixed (e.g. see [4]). As a result, the energy of the electronic quantum states and the corresponding electrostatic potential of the interacting nuclei, $U_n(R)$, depend on R. Since the dynamics of nuclei, in zero-order approximation, is ignored, the potential curves $U_n(R)$ remain the same for all isotopologues of hydrogen molecule (e.g. H_2, D_2, DT, etc.). The $U_n(R)$ terms in diatomic molecules are described by the projections of the total orbital angular momentum on the axis passing through the two nuclei, $\Lambda = 0, 1, \ldots$ (which are denoted with the Greek letters $\Sigma, \Pi, \ldots$) and the total spin of all electrons S (in the same way as in atoms). Finally, for the case where the atoms in the molecule are the same, the Hamiltonian is invariant with respect to the change of sign of the coordinates of all electrons and we can speak of the parity of electron wave functions, which can be even, denoted as "g" or odd, denoted as "u" (from corresponding German words

"gerade" and "ungerade"). Strictly speaking, we cannot apply this property for diatomic hydrogenic molecules composed of different isotopes. But in practice, the isotopic effect produces a very tiny impact (of the order of the electron to nucleon mass ratio [15]) on the energy spectrum, which, in practice, affects only the line radiation transport we will consider later. As a result, the molecular terms of all diatomic hydrogen molecules are practically identical to that of H_2, shown in Fig. II.3.

Once we know the potential $U_n(R)$, we can account for the dynamics of nuclei describing the rotational and vibrational quantum states [4]. For the background state of molecular hydrogen isotopologues, we can introduce the rotational energy as $U_{rot}(R) = E_{rot}K(K+1)$, where $E_{rot} = \hbar^2 / 2\tilde{M}R^2$, $\tilde{M}$ is the reduced mass of the nuclei and K is the quantum number (K=0, 1, 2, …) of the total angular momentum of the molecule. Then, using the potential $U_K(R) = U_n(R) + U_{rot}(R)$ and expanding $U_K(R)$ near the minimum at $R = R_{min}$ we can write

$$U_K(R) = U_K(R_{min}) + \frac{\tilde{M}}{2}\omega_v^2(\delta R)^2 \ , \qquad \text{(II.4)}$$

where $\delta R = R - R_{min}$ and $\omega_v^2 = \tilde{M}^{-1} d^2U_K(R)/dR^2\Big|_{R=R_{min}}$. The quantum mechanical motion of a particle in a quadratic potential gives the following expression for the energy of the vibrational quantum states: $E_v = \hbar\omega_v(v+1/2)$, where v is the vibrational quantum number (v=0, 1, 2, …). As a result, the energy terms of the diatomic molecule include three components: electronic, rotational, and vibrational, which gives

$$U_{tot}(R) = U_n(R) + E_{rot}K(K+1) + \hbar\omega_v(v+1/2) \ . \qquad \text{(II.5)}$$

The expression (II.5), where the contributions of vibrational and rotational states to the total energy are additive, is only valid for relatively low K and v values (e.g. see [4]), and for the higher ones their contributions are mixed. Therefore, the vibrational and rotational states are often called ro-vibrational states. Because the function $U_n(R)$ remains the same for all isotopologues of the hydrogen molecule, from the definition of E_{rot} and ω_v we find their dependences on the reduced mass of the nucleon: $E_{rot} \propto 1/\tilde{M}$, $\omega_v \propto 1/\sqrt{\tilde{M}}$, and for the H_2 molecule, $\hbar\omega_v = 0.54\,\text{eV}$ [4]. Different vibrational energy quanta for different isotopologues of the hydrogen molecule, but the same energy terms $U_n(R)$ and, therefore, the same dissociation energy of 4.48 eV, result in a different number of the available vibrational quantum states, which can be estimated as $v_{max} \propto \sqrt{\tilde{M}}$ (e.g. the H_2 molecule has $v_{max} = 14$).

In Fig. II.3, in addition to the molecular terms for H_2, are also shown the terms for the positive molecular ion, $H_2^{(+)}$, and the negative one, $H_2^{(-)}$. The latter is metastable with a relatively short natural life-time. However, it plays a crucial role in both the excitation of vibrational levels by electron impact $H_2(v) + e \to H_2^{(-)} \to H_2(v') + e$ and dissociative attachment $H_2(v) + e \to H_2^{(-)} \to H + H^-$ (e.g. see [12], [17], [18] and the references therein).

II.2 Collisional-radiative model

As we already mentioned, excited states of atoms and molecules in edge plasmas play important roles in virtually all atomic physics-related processes. Here, using the example of a hydrogen atom, we consider the basic physics of the CRM which is the main approach for a quantitative description of the processes the excited states can be involved in.

The population of excited states (for the simplest case of hydrogen-like ions, they correspond to $n > 1$) in edge plasma, depending on the plasma parameters, is determined by an interplay of electron impact excitation, electron transition from the continuum, radioactive decay, re-absorption of resonance photons, etc. We notice that for the energies relevant for the edge plasmas, the impact excitation of electronic and vibrational states by atoms and ions is usually negligible. Therefore, we start with a short review of electron-involved processes and their contributions to the rate equations governing the population of the excited states.

The binary interactions of particles, including electrons and heavy particles (atoms, molecules, and ions), are usually described by the effective cross-section, σ, of the particular process. In a very general case, σ depends on the relative speed of the interacting particles. Taking into account the large mass difference between the electrons and nuclei, for the case of electron interactions with atoms, molecules, and ions, the relative speed of the interacting particles is virtually equal to the electron speed. As a result, the cross-section of such interaction only depends on the electron kinetic energy, E_e. The cross-sections of many processes relevant for the edge plasmas are available from both quantum mechanical calculations and experiments (e.g. see [19], [20], [21] and the references therein). We notice that the cross-sections of the forward and reverse processes are related by the principle of detailed equilibrium (e.g. see [22]), so there is no need to calculate them separately.

As an illustration, we consider here the cross-sections of some electron-hydrogen interaction processes relevant to the population of excited states. For example, the cross-section of the electron impact excitation of the hydrogen atom from a level k to level n ($k < n$) can be written (e.g. see [23]) as

$$\sigma^{H}_{k\to n}(E_e) = \frac{128}{3^{3/2}Z^4}\left(\frac{\hbar^2}{m_e e^2}\right)^2 \frac{k^5 n^7}{(n^2-k^2)^5}\frac{\ell n(\varepsilon_e^{nk}+1)}{\varepsilon_e^{nk}+1} = \\ = \frac{32}{3^{3/2}}\left(\frac{e^2}{\Delta E_{nk}}\right)^2 \frac{k n^3}{(n^2-k^2)^3}\frac{\ell n(\varepsilon_e^{nk}+1)}{\varepsilon_e^{nk}+1}, \qquad \text{(II.6)}$$

where $\varepsilon_e^{nk} = (E_e - \Delta E_{nk})/\Delta E_{nk}$, $\Delta E_{nk} = E_k - E_n$ is the energy difference between the levels n and k, which gives for a hydrogen-like ion $\Delta E_{nk} \propto (k^{-2} - n^{-2})$. The cross-section for electron transition from continuum to hydrogen excited state n due to radiative recombination, $H^+ + e \to H(n) + \hbar\omega$ (where $E_e - E_n^H = \hbar\omega$, recall that E_n^H is negative), is given by the Kramers formula (e.g. see [12])

$$\sigma^{H}_{cont\to n}(E_e) = \frac{8\pi}{3^{3/2}(137)^2 n^3}\left(\frac{e^2}{E_e}\right)^2\left(1-\frac{E_n^H}{E_e}\right)^{-1}. \qquad \text{(II.7)}$$

Applying the classical Thompson formula for the hydrogen atom ionization cross-section from the excited state n, we find

$$\sigma_{ion}^{n}(E_e) \propto \left(\frac{e^2}{E_n^H}\right)^2 \frac{\left(\varepsilon_e^n - 1\right)}{\left(\varepsilon_e^n\right)^2}, \qquad \text{(II.8)}$$

where $\varepsilon_e^n = E_e / |E_n^H|$. Eq. (II.8) gives a good agreement with more sophisticated models (e.g. see [23]).

Interestingly, the dependences for electron impact excitation, radiative recombination, and ionization somewhat similar to Eq. (II.6)-(II.8) can be found from simple dimensional arguments. Indeed, the excitation (or ionization) cross-section, σ_{exc}, should depend on the electron energy E_e and the energy difference between the initial and final quantum states (including continuum) ΔE_{nk}. Therefore, the most general expression for σ_{exc} can be written as follows [3]

$$\sigma_{exc}^{k\to n}(E_e) = \left(\frac{e^2}{\Delta E_{nk}}\right)^2 f_{exc}^{k,n}(\varepsilon_e^{nk}), \qquad \text{(II.9)}$$

where the function $f_{exc}^{k,n}(x)$ ($f_{exc}^{k,n}(x<1)=0$) depends on some quantum mechanical particularities of the transition (e.g. on n and k). We notice that the scaling following from Eq. (II.9) works rather well for many inelastic processes ranging from neutral and ion ionization [3] to electron excitation (e.g. the electron impact excitation of hydrogen-like ions from n=1 to k=2 follows Eq. (II.9) for a wide range of Z [24]).

Eq. (II.9) predicts an important feature of the excitation and ionization cross-sections: their maximum values, which are $\sim\left(\Delta E_{nk}\right)^{-2}$, increase roughly $\sim n^4$ with increasing n. In addition, both the excitation and ionization energy thresholds decrease with increasing n, which increases the number of electrons that can contribute to these transitions. The latter circumstance is particularly important for low-temperature plasma, such that $T < I_H$. Finally, recalling Eq. (II.3), we see that the rate of spontaneous decay of highly excited states falls down. All these effects suggest an appreciable population of the excited states and emphasize the importance of these states in overall reaction rates (e.g. hydrogen ionization).

In other words, the so-called multistep processes including multiple excitation/de-excitation of atoms, molecules, and ions with following ionization, radiation, recombination and other processes affecting the population of excited states can significantly alter the rates of many atomic processes. They include not only ionization, recombination, and radiation loss, but also many other processes. Moreover, as we will see later, the presence of excited particles can "switch on" some important chemical reactions, which would not be possible otherwise.

To allow properly for the impact of the excited states on the rates of different atomic processes, one should consider the rate equations for the populations of these states. As an illustration, we consider here the rate equations for the excited states of a hydrogen atom. First, we should recall that the rate of a "reaction" (e.g. ionization) involving binary collisions between particles A and B can be written as $K_{AB}[A][B]$, where $[A]$ and $[B]$ are the densities of species

A and B and K_{AB} is the rate constant of this reaction, which can be expressed in terms of the cross-section of the process, $\sigma_{AB} \equiv \sigma_{AB}(|\vec{V}_A - \vec{V}_B|)$, as follows (e.g. see [22])

$$K_{AB} = \int d\vec{v}_A\, d\vec{v}_B \sigma_{AB}(|\vec{v}_A - \vec{v}_B|)\,|\vec{v}_A - \vec{v}_B|\, f_A(\vec{v}_A) f_B(\vec{v}_B) \left([A][B]\right)^{-1}, \qquad \text{(II.10)}$$

where $f_A(\vec{v}_A)$ and $f_B(\vec{v}_B)$ are the distribution functions of species A and B over velocity space normalized to their densities $[A]$ and $[B]$ (e.g. $\int d\vec{v}_A f_A(\vec{v}_A) = [A]$).

Being interested in binary collisions of electrons with "heavy" hydrogen atoms and protons, we can ignore the speed of the "heavy" particles in the expressions for the corresponding rate constants (II.10). As a result, the rate constants of electron-"heavy" particle interactions (e.g. electron impact excitation of the hydrogen atom $K^{(e)}_{k\to n}$) only include averaging over the electron distribution function $f_e(\vec{v},\vec{r},t)$:

$$K^{(e)}_{k\to n} n_e = \int \sigma^{(e)}_{k\to n}(v) v f_e(\vec{v},\vec{r},t)\, d\vec{v}, \qquad \text{(II.11)}$$

where $\sigma^{(e)}_{k\to n}(v)$ is the cross-section of the process under consideration. Thus, strictly speaking, in order to find the rate constant, one needs also allow for the evolution of the electron distribution function. However, today it is not feasible to use a fully kinetic approach for the study of all processes in the edge plasmas. Therefore with some exceptions, which will be considered in Ch. VI, edge plasma transport codes use a fluid approach where the distribution functions of the plasma particles are assumed to be shifted Maxwellian (applicability and limitations of this assumption will be considered in Ch. VI). Since the electron flow velocity in the edge plasma is much lower than the thermal electron speed, one can use in Eq. (II.11) the non-shifted Maxwellian electron distribution function. As a result, the rate constants of binary reactions involving electrons (e.g. $K^{(e)}_{k\to n}$) depend on the electron temperature T_e only.

For the case where the population of the excited states is due to electron impact and emission and reabsorption of photons, a symbolic form for the corresponding rate equations can be written as follows

$$\frac{d[H_n]}{dt} = -[H_n]\left\{ n_e \sum_{k\neq n} K^{(e)}_{n\to k} + \sum_{k\neq n} \nu^{(rad)}_{n\to k} \right\} + \sum_{k\neq n} K^{(e)}_{k\to n}[H_k] n_e + \sum_{k\neq n} \nu^{(rad)}_{k\to n}[H_k] + \sum_{k\neq n} S^{(rad)}_n + S^{(transp)}_n, \qquad \text{(II.12)}$$

where $[H_n]$ and n_e are the densities of hydrogen atoms in the quantum state n and electrons respectively; $K^{(e)}_{k\to n}$ is the rate constant of electron-induced transition from the state k to the state n; $\nu^{(rad)}_{k\to n}$ is the effective frequency of spontaneous decay of the state k to the state n. $S^{(rad)}_n$ and $S^{(transp)}_n$ are the sources and sinks of the population of different quantum states, caused by photon absorption and transport of atoms, respectively (we notice that the states k can also include continuum).

Examining different terms in Eq. (II.12), one finds that for the edge plasma conditions, the characteristic equilibration time of the population of excited states (described by the first term on the right-hand side of Eq. (II.12)) is usually much shorter than the characteristic times of

i) variation of the hydrogen density in the ground state, $|d\ell n[H_1]/dt|^{-1}$ and ii) transport of exited states described by the last term in Eq. (II.12). As a result, the population of all electronically excited states in a hydrogen atom can be considered in a local quasi-steady approximation assuming that $[H_1]$ and the plasma density and temperatures are fixed. A similar approximation is often used for chemical radicals in theoretical models of chemical reactions (see [5], [6] and the references therein). The equations following from this approximation, that greatly simplifies the rate equations for the population of excited states, are called the Collisional-Radiative Model. Originally it was developed for hydrogen, and then extended to helium, impurities, and molecular hydrogen (e.g. see [25], [26], [13], [27], [28] [29], [30], [31], [12] and the references therein).

The CRM can be simplified further by using proximity of the states with $n \approx n_{max}$ to continuum and describing their population by the local thermodynamic equilibrium (LTE) by implementing the Saha equilibrium, so that $[H_{n_{max}}] \propto [H^+]n_e$, (see [25], [26], [29], [13], [5], [12] and the references therein). Moreover, since in edge plasmas $[H_1] >> \sum_{n=2}^{n=n_{max}} [H_n]$, we can assume that $[H_1]$ equals to the density of atomic hydrogen $[H]$. As a result, we arrive at the set of linear algebraic equations for the population of quantum states $1 < n < n_{max}$:

$$0 = -[H_n]\left\{\sum_{k=1,k\neq n}^{n_{max}} n_e K^{(e)}_{n\to k} + n_e K^{(ion)}_{n\to cont} + \sum_{k=1}^{n-1} \nu^{(rad)}_{n\to k}\right\} + \sum_{k=1,k\neq n}^{n_{max}} n_e K^{(e)}_{k\to n}[H_k] + \sum_{k>n}^{n_{max}} \nu^{(rad)}_{k\to n}[H_k] + K^{(rec)}_{cont\to n}[H^+]n_e + \sum_{k\neq n} S^{(rad)}_n \quad , \qquad \text{(II.13)}$$

where the rate constants $K^{(ion)}_{n\to cont}$ and $K^{(rec)}_{cont\to n}$ describe ionization and radiative recombination from the continuum. Recalling that $[H_{n_{max}}] \propto [H^+]n_e$, we find that the solution of Eq. (II.13) can be expressed as a linear combination of the density of atomic hydrogen $[H]$, the product $[H^+]n_e$, and a term describing radiation-induced transitions $S^{(rad)}_n$. Neglecting, for simplicity, the $S^{(rad)}_n$ terms, we have

$$[H_n] = \xi^H_n [H] + \xi^{H^+}_n [H^+]n_e, \qquad \text{(II.14)}$$

where the functions ξ^H_n and $\xi^{H^+}_n$ can be found from the solution of corresponding sub-sets of Eq. (II.13) in terms of the electron and hydrogen ion densities and the rate constants and the frequencies of radiative decay $K^{(e)}_{n\to k}$, $K^{(ion)}_{l\to cont}$, $\nu^{(rad)}_{n\to k}$, and $K^{(rad)}_{cont\to n}$. Substituting expression (II.14) into the equation for the population of the ground state, from (II.12) we find

$$\frac{d[H]}{dt} = -\left\{ K_{1\to cont}^{(ion)} + \sum_{k=2}^{n_{max}} K_{k\to cont}^{(ion)} \xi_k^H \right\} [H] n_e + \left\{ K_{cont\to 1}^{(rec)} + n_e \sum_{k=2}^{n_{max}} K_{k\to 1}^{(e)} \xi_k^{H^+} + n_e^{-1} \sum_{k=2}^{n_{max}} \nu_{k\to 1}^{(rad)} \xi_k^{H^+} \right\} [H^+] n_e + S_H^{transp}, \quad \text{(II.15)}$$

where the first and second terms on the right-hand side of Eq. (II.15) can be interpreted as the hydrogen ionization and electron-ion recombination (EIR) rates (including both radiative and three-body recombination). Accordingly, the expressions in the first and second braces on the right-hand side of Eq. (II.15) are called the hydrogen ionization, K_{ion}^H, and electron-ion recombination (EIR, which includes both radiative and three-body recombination processes), K_{rec}^H, rate constants. As a result, we can re-write Eq. (II.15) as follows

$$\frac{d[H]}{dt} = -K_{ion}^H n_e [H] + K_{rec}^H n_e [H^+] + S_n^{(transp)}. \quad \text{(II.16)}$$

The CRM is widely used in the modeling of gas discharge, fusion, and astrophysical plasmas (e.g. see [25], [13], [27], [28] [29], [30], [31], [12], [23] and the references therein). It is much simpler than the time-dependent rate equations (II.12) whereas allowing for the impact of excited states on both the ionization and recombination processes. We notice that since the population of excited states is established in a competition of electron-induced transitions and spontaneous decays, both rate constants K_{ion}^H and K_{rec}^H depend on the electron density and temperature. However, in optically thick plasma, re-absorption of resonance photons (in fusion plasmas they are usually Ly_α and Ly_β) can alter the population of the excited states (recall terms $S_n^{(rad)}$ in Eq. (II.13)) and, therefore, the ionization and recombination rate constants.

We will see below that because of high ionization rates of the excited states, the multistep processes including excitation and quenching of the excited hydrogen levels result, at sufficiently high plasma density, in a significant increase of the effective hydrogen ionization rate constant. Moreover, even the constants of elastic processes involving excited states can depend on n. In particular, the rate $K_{cx}^{(n)}$ of the so-called charge exchange process, $H(n) + H^+ \to H^+ + H(n)$, increases with increasing n and is proportional, although approximately, to n^4 [32]. Such elastic collisions play a vital role in plasma-neutral momentum exchange and divertor detachment physics (e.g. see [33] and the references therein). Therefore, a correct assessment of the impact of excited states on overall momentum exchange is important.

A crude estimate of the effective resonance charge exchange rate constant, based on a simple averaging of corresponding cross-sections over relative population of excited states, similar to that of the ionization rate constant, $\bar{K}_{cx} = \sum_n K_{cx}^{(n)} [H_n]/[H]$, demonstrates a significant increase of $\bar{K}_{cx}$ in comparison to the cross-section involving hydrogen in the ground state, $K_{cx}^{(1)}$ [34]. If this simple estimate held, it would imply an important impact on both hydrogen transport and plasma-neutral coupling described with both Monte Carlo codes and fluid models (e.g. see [35]). However, more thorough consideration shows that such a simplified

description of the contribution of the excited states to hydrogen transport and plasma-neutral momentum exchange is incorrect [36].

For a proper consideration of ion-neutral momentum exchange we need to consider the distribution functions of protons, $f_i(\vec{v})$, and atoms in all excited states, $f^H_{(n)}(\vec{v})$. Then, since the charge-exchange cross-section of excited states is much higher than that of the ground state, recall $K^{(n)}_{cx} \propto n^4$, we can assume that not only the density of the excited states (as it is considered within CRM) but also their velocity distribution functions $f^H_{(n)}(\vec{v})$ can be treated in a quasi-equilibrium approximation leaving only a relatively slow variation of density and distribution function of the ground state. Then we can write the following counterparts of Eq. (II.13) and (II.15) for the distribution functions $f^H_{(n)}(\vec{v})$ allowing, in addition to electron-neutral interactions and spontaneous decays of excited states, for the charge-exchange processes:

$$0 = -f^H_{(n)}(\vec{v})\left\{\sum_{k=1,k\neq n}^{n_{max}} n_e K^{(e)}_{n\to k} + n_e K^{(ion)}_{n\to cont} + \sum_{k=1}^{n-1} \nu^{(rad)}_{n\to k}\right\} + \sum_{k>n}^{n_{max}} \nu^{(rad)}_{k\to n} f^H_{(k)}(\vec{v}) + \sum_{k=1,k\neq n}^{n_{max}} n_e K^{(e)}_{k\to n} f^H_{(k)}(\vec{v}) - K^{(n)}_{cx}\left\{n_i f^H_{(n)}(\vec{v}) - [H_n] f_i(\vec{v})\right\}, \quad \text{(II.17)}$$

and

$$\frac{df^H(\vec{v})}{dt} = -n_e\left\{\sum_{k=2}^{n_{max}} K^{(e)}_{1\to k} + K^{(ion)}_{1\to cont}\right\} f^H(\vec{v}) + \left\{\sum_{k=2}^{n_{max}} \left(n_e K^{(e)}_{k\to 1} + \nu^{(rad)}_{k\to 1}\right) f^H_{(k)}(\vec{v})\right\} - K^{(1)}_{cx}\left\{n_i f^H(\vec{v}) - [H] f_i(\vec{v})\right\}, \quad \text{(II.18)}$$

where n_i is the proton density, $f^H(\vec{v}) \equiv f^H_{(1)}(\vec{v})$, $df^H(\vec{v})/dt = \partial f^H(\vec{v})/\partial t + \vec{v}\cdot\nabla_{\vec{r}} f^H(\vec{v})$. For simplicity, we assume that $\sigma^{(n)}_{cx}(v)v \equiv K^{(n)}_{cx}$ does not depend on the velocity v and neglect all free-to-bound transitions (i.e. recombination processes), which assumes the electron temperature corresponding to "ionizing" plasma. We notice the integration of Eq. (II.17)–(II.18) over the velocity space brings us back to Eq. (II.13) and (II.15) and, therefore, to the following relation $[H_n] = \int d\vec{v} f^H_{(n)}(\vec{v})$, with $[H_n]$ given by the CRM. To find $f^H_{(k)}(\vec{v})$ we observe that the solution of Eq. (II.17) depends only on $f_i(\vec{v})$ and $f^H(\vec{v})$. Then, following [37], we can write the functions $f^H_{(n)}(\vec{v})$ as $f^H_{(n)}(\vec{v}) = [H_n]\left\{\delta_n f_i(\vec{v})/n_i + (1-\delta_n) f^H(\vec{v})/[H]\right\}$, where δ_n are the partition coefficients. Substituting this expression for $f^H_{(n)}(\vec{v})$ into Eq. (II.17)–(II.18), we obtain algebraic equations for δ_n, which are somewhat similar to the equations (II.13) but allowing also for charge exchange processes of the atoms on excited states:

$$0 = -[H_n]\delta_n \left\{ \sum_{k=1,k\neq n}^{n_{max}} n_e K_{n\to k}^{(e)} + n_e K_{n\to cont}^{(ion)} + \sum_{k=1}^{n-1} \nu_{n\to k}^{(rad)} + K_{cx}^{(n)} n_i \right\},$$
$$+ \sum_{k>n}^{n_{max}} \nu_{k\to n}^{(rad)} [H_k]\delta_k + \sum_{k=1,k\neq n}^{n_{max}} n_e K_{k\to n}^{(e)} [H_k]\delta_k + K_{cx}^{(n)} n_i [H_n] \quad \text{(II.19)}$$

and the following equation for the evolution of the function $f^H(\vec{v})$:

$$\frac{df^H(\vec{v})}{dt} = -K_{ion}^H n_e f^H(\vec{v}) - K_{cx}^H \left\{ n_i f^H(\vec{v}) - [H] f_i(\vec{v}) \right\}, \quad \text{(II.20)}$$

where the first term on the right-hand side of Eq. (II.20) describes just the effective ionization rate constant, recall Eq. (II.16), and

$$K_{cx}^H = K_{cx}^{(1)} + \sum_{k=2}^{n_{max}} n_i^{-1} \left(n_e K_{k\to 1}^{(e)} + \nu_{k\to 1}^{(rad)} \right) \delta_k \left([H_k]/[H] \right), \quad \text{(II.21)}$$

is the effective charge exchange rate constant taking into account the contribution of the excited states. As we see, the structure of the expression (II.21) is very different from effective charge exchange cross-section accounting for the contribution of excited states $\bar{K}_{cx} = \sum_n K_{cx}^{(n)} [H_n]/[H]$ suggested in Ref. [34].

By adopting Grad expansion of both the neutral and ion distribution functions (see Ch. VI for details), it is possible to extend the analysis of the role of excited states to a very general hydrogen-ion elastic collision operator (including the charge-exchange one). However, it goes beyond our simple demonstration of the possible extension of the CRM to the evaluation of an impact of the excited states on elastic collisions and neutral transport. Calculations performed in [37] have shown that in a contrast to the results from [34], K_{cx}^H exceeds $K_{cx}^{(1)}$ by only 10-15% and an impact of the excited states on neutral hydrogen transport is not very important. This is because of: i) the comparability of the magnitude of $K_{cx}^{(1)}$ to the electron impact excitation rate constant of the hydrogen atom, and ii) fast transition from excited to the ground state. However, the conclusion of the importance of electron exchange recombination of an impurity ion in the course of the interactions with excited hydrogen atoms [34] largely holds because hydrogen in the ground state does not undergo such a "resonance" charge exchange process.

The application of the CRM to impurity atoms/ions and molecules results in more complex equations than Eq. (II.13), Eq. (II.15). This is because i) the number of states, which should be considered within CRM for each individual atom/ion, increases; ii) few ionization states of the same kind of atom/ion can exist for given plasma density and electron temperature; iii) the population of excited states of impurity atom/ion in edge plasma can be affected by charge-exchange process involving hydrogen atoms (e.g. $A^{Z+1} + H \to A^Z(n) + H^+$, where A^Z and $A^Z(n)$ are impurity atoms in ionization states Z+1 and excited level of ionization state z) [21]; iv) the so-called dielectronic recombination process (accompanied by excitation of an ion's electron and formation of a doubly excited atom/ion with subsequent emission of the photon, $A^{Z+1} + e \to A^Z(n,n') \to A^Z + \hbar\omega$) should be considered (e.g. see [38], [39] and the references

therein); and v) some excited quantum states of complex atoms/ions are "metastable" or just stable (e.g. the ro-vibrational states of hydrogenic molecules).

To take into account such processes, one needs to modify the rate equations (II.12) adding some new terms (for example, quenching of metastable states on vacuum chamber walls, which becomes important in weakly ionized plasma (e.g. see [13]). This means that in such plasmas, one should consider the transport terms for the particle density not only in the ground state but also in the metastable states. However, in relatively high density and rather hot fusion plasma, an effective lifetime of the metastable states is determined largely by the interactions of the metastable atoms/ions with electrons and is strongly reduced in comparison to their natural lifetime. In addition, the natural lifetime of ionic metastable states is decreasing as Z^{-8} with increasing the ion charge Z. We also remind that some quantum states within the "thin structure" of the hydrogen energy levels, caused by relativistic effects, are also metastable. But due to the strong "mixing" of these levels in a fusion plasma environment, these metastable states play no significant role. As a result, in fusion research the transport of metastable states is usually ignored and their populations (as well as ionization/recombination balance and radiation loss) are considered in a quasi-equilibrium approximation (recall Eq. (II.13)) on the equal footage with other excited states (e.g. for details see [30] and the references therein). The results of comprehensive numerical modeling show that for the edge plasma conditions, even the metastable state 2^3S_1 of helium, having the lifetime $\sim 10^4$ s, can be treated in quasi-equilibrium approximation [40]. The presently most advanced database providing the fusion-relevant impurity radiation loss, the contribution of different lines, the rate constants, etc., is the ADAS database [41]. The divertor modeling codes whose development had started before the ADAS database became the de-facto standard can use some other data sources (for example, the AMJUEL, HYDHEL and METHANE data sets [42] in SOLPS).

II.3 Line radiation transport in edge plasma

As we have seen in the previous sub-section, the populations of excited states are determined by the competition between the processes involving interactions with electrons and, playing important role, radiative decays (e.g. from level n to level k), which are accompanied by the emission of photons having the energy $\hbar\omega_0 \approx \Delta E_{nk}$, where ω_0 is the photon frequency corresponding to the decay $n \to k$. This is the so-called "line radiation", which dominates in edge plasmas. However, in our simplified analysis of the CRM for hydrogen atoms, (recall Eq. (II.13)), we neglected the term $S_n^{(rad)}$ describing inter-state transitions stimulated by the photons. These two features of our analysis could only be reconciled for the case of so-called "transparent" media, where the effective mean free path of a photon to absorption by a neutral/ion, ℓ_{abs}, is longer than the characteristic scale-length, L, (e.g. for the case of radiation in the divertor volume, it could be the poloidal width of divertor). An opposite case, where $\ell_{abs} < L$, is called the "opaque" or "optically thick" one.

Since the photon absorption rate is proportional to the density of available absorbers, and absorption process in edge plasma largely has a resonant nature (recall the relation $\hbar\omega_0 \approx \Delta E_{nk}$), edge plasma can be transparent for the radiation corresponding to some lines and opaque for the other ones (the latter case is often referred to as radiation "trapping"). Because the density of hydrogen atoms (hydrogen molecules are dissociated rather quickly due to electron impacts) is

the largest among the radiating species in the edge plasma, the line radiation related to atomic hydrogen is the first candidate for being trapped. Moreover, since the majority of atomic hydrogen is in the ground state, the most strongly "trapped" hydrogen lines are Ly_α and Ly_β, related, respectively, to the transitions $n = 2 \rightarrow k = 1$ and $n = 3 \rightarrow k = 1$ (we will see that the absorption of other lines in Lyman series is weaker due to reduction of corresponding oscillator strengths). It was shown (e.g. see [43], [44]) that trapping effects for Ly_α and Ly_β lines become important already for current tokamaks and they are expected to be much more pronounced in the future tokamak reactors (e.g. ITER [45]).

As one could notice, we have stated that the frequency of the emitted photon ω_0 is only approximately equal to $\Delta E_{kn}/\hbar$. The reason for this is the so-called line "broadening", which results in the fact that emitted photons have some frequency distribution, described by the "line shape" function, $a(\omega)$ (localized around ω_0 and having characteristic width $\Delta\omega << \omega_0$), such that $\int a(\omega)d\omega = 1$. There are few reasons for line broadening in edge plasma. First, there is a "natural" broadening of the line, Γ, caused by the finite time of the radiation emission, which corresponds to the decay rate of the excited state determined by the Einstein coefficients (II.2). However, in practice $\Delta\omega$ is, in most cases, much larger than Γ. In edge plasma both $\Delta\omega$ and the shape of the function $a(\omega)$ are largely determined by i) Doppler broadening related to the shift of the frequency of the radiation emitted by moving particles, so that $\Delta\omega_D \sim \omega_0(V_{th}/c)$, where V_{th} is the particle thermal speed; ii) Stark broadening due to the micro-electric fields $E_{micro} \sim en_e^{2/3}$, causing a change in the energy of the quantum states and yielding, for a hydrogen atom, $\Delta\omega_S \sim (\hbar/m_e e)E_{micro}$; iii) Zeeman effect that results, in the presence of a large magnetic field, in splitting the quantum states; and, finally, iv) the so-called motional Stark effects related to the effective electric field, $E_B \sim (V_N/c)B$. (e. g. see [46], [47], and the references therein).

For the case where the line width is only determined by the decay rate, the effective cross-section of absorption of a resonant photon, $\sigma_{abs}(\omega_0)$, is proportional to the square of the photon wavelength, i.e. $\sigma_{abs}(\omega_0) \sim (c/\omega_0)^2$. We note that for the edge plasma conditions, $\omega_0 >> \omega_{pe} \equiv \sqrt{4\pi n_e e^2/m_e}$, where ω_{pe} is the Langmuir frequency, so one can neglect plasma effects in the dispersion of the line radiation and take $\omega_0 = k_0 c$, where k_0 is the photon wavenumber. However, broadening of the line, such that $\Delta\omega >> \Gamma$, results in a strong reduction of $\sigma_{abs}(\omega_0)$, which now becomes $\sim (c/\omega_0)^2(\Gamma/\Delta\omega)$. For example, for the case where the Doppler effect dominates the line broadening, the characteristic absorption length of the line corresponding to the transition between the n-th excited state and the ground one in a hydrogen atom, $\ell_{abs} \sim 1/\sigma_{abs}(\omega_0)[H]$, can be found from the following expression [20]

$$\ell_{abs} = \left\{ \pi^{3/2} \left(c / \omega_{1n} \right)^2 \left(n^2 A^H_{n \to 1} / \Delta\omega_D \right) [H] \right\}^{-1}, \qquad \text{(II.22)}$$

where $\omega_{1n} = \Delta E_{1n} / \hbar$, $\Delta\omega_D = \omega_{1n} (2T_{[H]} / M_{nucl})^{1/2} / c$, and $T_{[H]}$ is the temperature of the hydrogen atoms. For $[H] = 10^{14} cm^{-3}$ and $T_{[H]} = 3\,eV$, which are rather typical for dense divertor plasma, from Eq. (II.22) we find the absorption lengths of Ly_α ~0.2 cm and Ly_β ~2 cm, which is shorter than the characteristic scale-length of the variation of the neutral gas density and one can expect trapping of both Ly_α and Ly_β radiation.

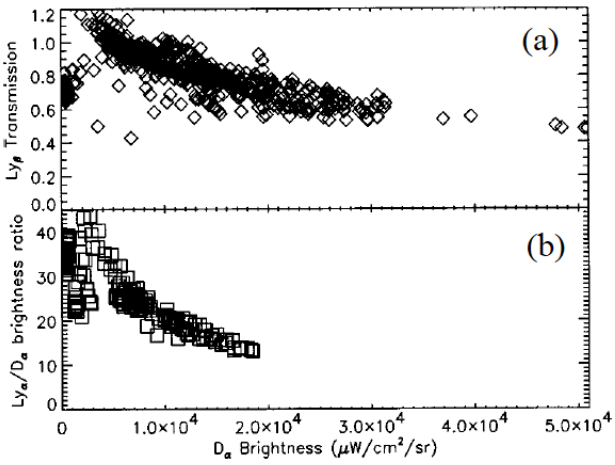

Fig. II.4. The dependences of the Ly_β transmission (a) and the intensity of Ly_α (b) on the intensity of D_α. Reproduced with permission from [48], © AIP Publishing 1998.

The radiation trapping alters the partition of radiation in different line series (e.g. Lyman and Balmer series). For example, in a transparent plasma, the partition of Ly_β (transition $3 \to 1$) and H_α (transition $3 \to 2$) intensities depends only on the corresponding spontaneous emission coefficients and their ratio should remain constant. However, if Ly_β is trapped (H_α is not trapped in the edge plasma due to a very small ratio $[H_{n=2}]/[H]$), this partition will change, which exhibits a clear signature of the radiation trapping effects. Such a change in Ly_β and H_α partition was, in particular, observed in experiments on Alcator-C-Mod tokamak [48] and can be seen in Fig. II.4a, where the Ly_β intensity decreases with increasing D_α intensity (D_α is the line $3 \to 2$ in deuterium). We note that the increase of D_α intensity at the same plasma temperature implies the increase of the atomic hydrogen density. In addition, in Fig. II.4b we see that the intensity of Ly_α decreases also with increasing D_α intensity, implying Ly_α radiation trapping. These results are consistent with the expression (II.22), which predicts that the trapping effects become more pronounced with increasing hydrogen density.

So far, in this subsection, we did not distinguish between the hydrogen isotopes. However, in practice, the expression (II.1) has some correction $\sim m_e / M_{nucl}$ caused by the finite electron to the nucleus, M_{nucl} , mass ratio. It causes the isotope-dependent shift, $\Delta\omega_{nucl} \approx \omega_0 (m_e / M_{nucl}) \sim 3 \times 10^{-4} \omega_0$, of the resonance frequencies ω_0 . But, for typical neutral hydrogen temperature ~ few eV we have $\Delta\omega_D \sim 3 \times 10^{-5} \omega_0 << \Delta\omega_{nucl}$. This implies small overlapping of corresponding line shapes a(ω) of different isotopes and weak interference of their line radiation transport. However, at high plasma density, Stark broadening could exceed

the Doppler one and overlapping of the lines could be much stronger.

In our estimates related to both absorption length of line radiation and interference of line radiation emitted by different hydrogen isotopes, we have used rather crude models where the details of the line shape $a(\omega)$ were ignored. As a matter of fact, in these models, we focused on the transport of photons corresponding to the "center" of the line. However, for the case where the photons having the frequency close to the line center are trapped and, therefore, their transport is impaired, the main contribution to energy transport via line radiation will come from the "wings" of the line shape [49], [50], [12]. To include the impact of different line broadening mechanisms, the Voigt line shape, $a(\tilde{\omega}) = V(\tilde{\omega},\sigma_\omega,\gamma)$, which is the convolution of the Gaussian profile, $G(\tilde{\omega},\sigma_\omega) = \exp\left(-\tilde{\omega}^2/2\sigma_\omega^2\right)/\sigma_\omega\sqrt{2\pi}$, (accounting for Doppler broadening) and Lorentzian profile, $L(\tilde{\omega},\gamma) = \pi^{-1}\gamma/(\tilde{\omega}^2+\gamma^2)$, (describing, to some approximation, the Stark effect),

$$V(\tilde{\omega},\sigma_\omega,\gamma) = \int_{-\infty}^{\infty} G(\tilde{\omega}',\sigma_\omega)L(\tilde{\omega}-\tilde{\omega}',\gamma)\,d\tilde{\omega}', \qquad \text{(II.23)}$$

where $\tilde{\omega} = \omega - \omega_0$, whereas σ_ω and γ are the characteristic widths of the Gaussian and Lorentzian profiles, respectively. Although the Voight approximation is often used in simplified models, more detail calculations show (e.g. [51], [40]) that Zeeman splitting (which is not included in the expression (II.23)) can play an important role in edge plasma radiation transport.

In order to describe properly the line radiation trapping effects on both the energy loss and the atomic physic processes, one needs to consider the photon kinetic equation (e.g. see [49], [50], [12] and the references therein). Here, just for illustration, we consider the case where the radiation trapping is important for a particular line corresponding to the transition in the atom "D" from a quantum level with high energy ("u") to the lower one ("d"). First, we introduce the radiant intensity per solid angle, $I_\omega(\vec{r},\vec{\Omega})$, which depends on the spatial coordinate $\vec{r}$ and the photon propagation direction in the solid angle $\vec{\Omega}$. Then, assuming: i) steady-state approximation for $I_\omega(\vec{r},\vec{\Omega})$ and ii) that the absorption and emission line shapes are described by the same isotropic function $a(\omega)$, we arrive at the following equation:

$$\frac{4\pi}{\hbar\omega}\vec{c}\cdot\nabla I_\omega = a(\omega)\left(A_{u,d}[D_u] + I_\omega B_{u,d}[D_u] - I_\omega B_{d,u}[D_d]\right), \qquad \text{(II.24)}$$

where $[D_{(...)}]$ are the densities of atoms in the high and low energy states; $\vec{c}$ is the photon velocity vector; $B_{d,u}$, $B_{u,d}$, and $A_{u,d}$ are the Einstein coefficients

$$B_{u,d} = A_{u,d}\frac{4\pi^3c^2}{\hbar\omega^3}, \qquad B_{d,u} = \frac{g_u}{g_d}B_{u,d}, \qquad \text{(II.25)}$$

$g_{(...)}$ is the statistical weight of the state (…), and $A_{u,d}$ can be found from quantum mechanics (e.g. for hydrogen atom it is determined by Eq. (II.2)).

The terms in the brackets on the right-hand side of Eq. (II.24) describe, respectively, spontaneous and induced emission of the photons and photon absorption. For edge plasmas, induced emission is small and can be neglected. By integrating the photon absorption term we find the source for the population of the "u" quantum state caused by absorption of the radiation

by atoms in the "d" quantum state, $S_u^{(rad)} = (4\pi)^{-1} \int a(\omega) I_\omega \, d\omega \, d\vec{\Omega} B_{d,u}[D_d]$, which enters in Eq. (II.13) for the population of excited states.

We note that in edge plasmas, atom densities and the line shape function depend on the spatial coordinate. The latter feature makes it extremely difficult to find reliable estimates of radiation transport [50], [12]. In addition, the radiation trapping modifies the rates of the atomic processes (recall Eq. (II.13) and, therefore, the population densities appearing in Eq. (II.24). Thus, we see that both radiation transport and the dynamics of the population of excited states of atomic hydrogen become coupled. Moreover, since the emission of a photon can happen in one region and its absorption in another one, the synergistic effects of radiation transport and atomic processes appear to be non-local.

As a result, except very crude models that will be discussed later, realistic solutions of these complex coupled problems could only be found numerically.

At this moment, the most advanced numerical package capable of treating both the atomic physics and radiation transport effects in complex edge plasma geometry is built into the EIRENE Monte Carlo code (e.g. see references [52], [53], [40]). Another multi-dimensional code which was used for the radiation transport modeling in edge plasma is Cretin [54], [51], [55], [56]. The results of the simulations performed with both EIRENE and Cretin show a reasonably good agreement.

Modeling of the JET, Alcator-C-Mod, and ITER plasmas with EIRENE shows that radiation transport plays a crucial role in hydrogen ionization processes in optically thick (large product of the hydrogen atom density and the spatial scale length) devices. For example, while in JET, the radiation-stimulated ionization contributes only 10-20% to the total ionization source, in more optically thick Alcator-C-Mod this number increases to 30%, and in ITER, depending on the regime, it rises to 60-90% [40]. Unfortunately, self-consistent modeling of radiation transport and the atomic physics effects is very computationally expensive, so that in many cases the radiation trapping effects are ignored. Partly it is justified by the fact that some features important for the reactor design, such as the heat load on divertor targets, appear to be quite insensitive to the outcome of the radiation trapping effects (e.g. see [53]. However, these effects appear to be crucial for proper modeling of some particular phenomena observed in experiments (e.g. modeling of MARFE in JET tokamak where it was found that 90% of Ly_α and 70% of Ly_β lines are trapped [57]) and they are also often important for interpretation of the diagnostic (e.g. spectroscopic) data [48].

II.4 Application of CRM to edge plasma relevant species

In this sub-section, we consider the results of the application of the CRM to different atomic and molecular species relevant to the edge plasma in magnetic fusion devices.

II.4.1 Hydrogen

We start with hydrogen atoms and molecules. An impact of radiation trapping on the atomic rate constants of hydrogen species, in general, depends on the particular distribution of the plasma and neutral gas parameters. However, just to taste a flavor of the radiation trapping effects, one can consider a model where hydrogen radiation in some particular lines is completely trapped.

This case corresponds to a CRM where spontaneous decay from some particular quantum states is turned off, which mimics quick reabsorption of the resonance photons [26].

In Fig. II.5, one can find the dependence of both the atomic hydrogen ionization K_{ion}^{H} and the EIR K_{rec}^{H} rate constants on the temperature for different plasma densities for the case of fully transparent plasma (Fig. II.5a) and suppressed spontaneous decay from the levels $n \geq 2$ to the ground state (Fig. II.5b), which mimics the complete opacity conditions for the Lyman lines, obtained from the SOLPS database [42].

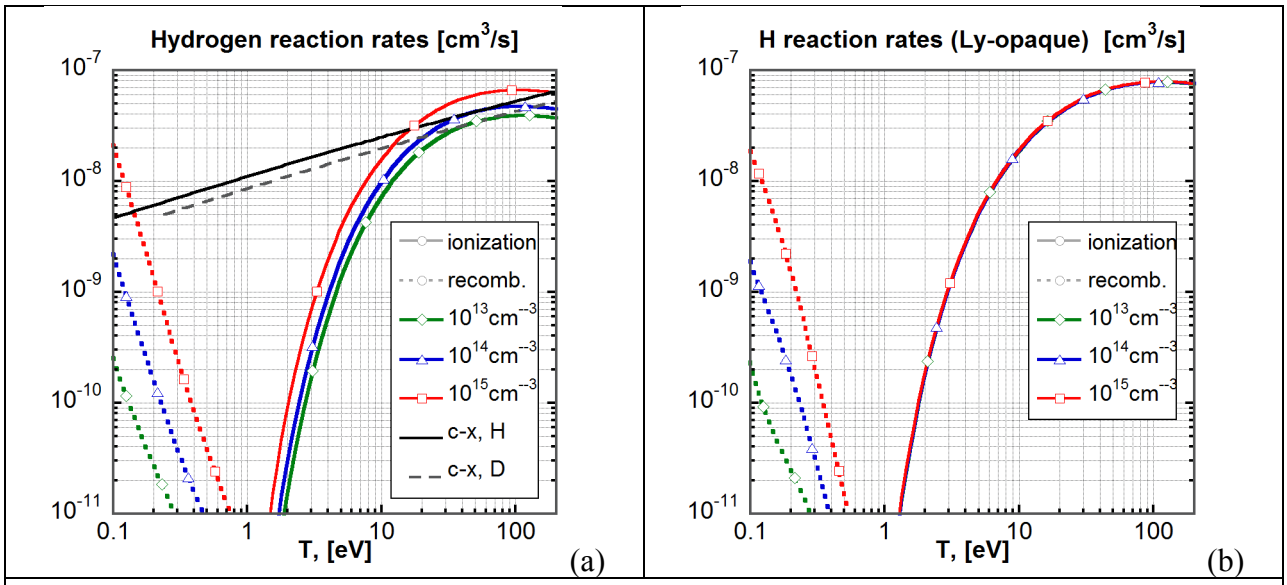

Fig. II.5. Dependence of the hydrogen ionization, K_{ion}^{H}, and EIR, K_{rec}^{H}, rate constants on the electron temperature for different electron densities for the case of fully transparent plasma (Fig. II.5a) and suppressed spontaneous decay from the levels $n \geq 2$ to the ground state (Fig. II.5b), which mimics the complete opacity conditions for the Lyman lines. In Fig.II.5a the charge-exchange rate constant $K_{cx}^{(1)}$ is shown for different hydrogen isotopes assuming that the electron/ion/neutral temperatures are equal.

As one could expect, both the increase of the electron density above $\sim 10^{14}\,cm^{-3}$ and the suppression of the spontaneous decay of the transition $2 \rightarrow 1$, which enhance the population of excited states, are boosting the ionization rate constant. In Fig. II.5a we also plot the charge-exchange rate constants $K_{cx}^{(1)}$ (which will be used for our further considerations) for different hydrogen isotopes assuming that the electron and ion/neutral temperatures are the same. However, in practice, the analysis of edge plasma and neutral hydrogen transport requires more detailed knowledge of the elastic collisions involving the ions, atoms, and molecules of the hydrogenic species. The relevant cross-sections (including momentum and charge transfer) can be found from both semi-classical and fully quantal calculations (e.g. see [58], [59]).

Both the ionization and recombination rates are necessary for the evaluation of the plasma recycling processes. However, the ionization of neutrals, which is accompanied by neutral gas excitation and following radiation, results in plasma energy dissipation. Thus, as it

was noted in Ch. 1, to maintain plasma recycling, the recycling region must be supplied with power.

To assess the energy dissipation caused by plasma recycling, it is convenient to introduce the hydrogen "ionization cost" [60], E_{ion}^{H}, which corresponds to plasma energy dissipation per an ionization event:

$$E_{ion}^{H} = \left\{ \sum_{n} [H_n] \left(-E_n K_{n\to cont}^{(ion)} n_e + \sum_{k<n} \Delta E_{nk} \nu_{n\to k}^{(rad)} \right) \right\} \left([H] n_e K_{ion}^{H} \right)^{-1}, \qquad \text{(II.26)}$$

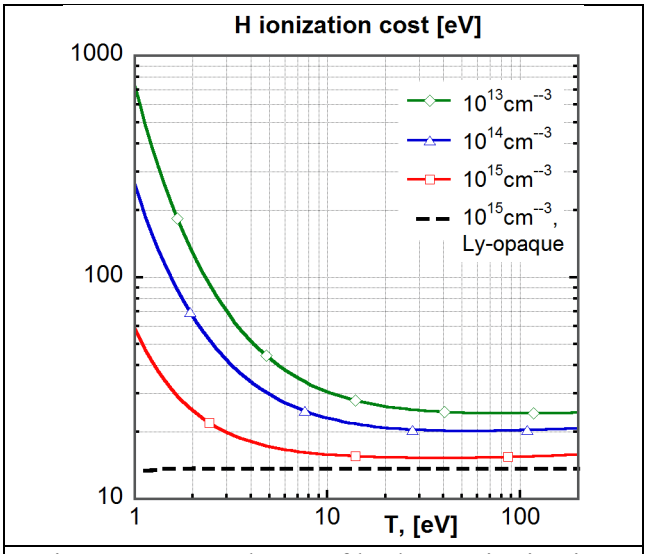

Fig. II.6. Dependence of hydrogen ionization cost E_{ion}^{H} on electron temperature for different plasma densities for the case of fully transparent plasma and suppressed spontaneous decay from the levels $n \geq 2$ to the ground state, which mimics completely opaque condition for Lyman lines.

where the population of excited states is taken from the CRM. It is obvious that E_{ion}^{H} depends on the electron temperature and density and is significantly altered by the radiation trapping effects. As an example, the dependence of E_{ion}^{H} on T_e for different electron densities is shown in Fig. II.6 for the cases of transparent plasma and suppressed spontaneous decay from the levels $n \geq 2$ to the ground state (Fig. II.6b), which corresponds to the complete opacity conditions for Lyman lines radiation.

As we see from Fig.II.6, E_{ion}^{H} is around 30 eV and even higher for the transparent and not so dense ($n_e < 10^{14} cm^{-3}$) plasma, which significantly exceeds the hydrogen ionization potential $I_H = 13.6\,eV$ since the excitation rate constants exceed the ionization ones. However, E_{ion}^{H} falls with increasing electron density above $\sim 10^{14} cm^{-3}$ to the values close to $I_H = 13.6\,eV$ due to the contribution of the multi-step processes to ionization even for transparent plasma. This effect becomes more pronounced for the plasma opaque for the Lyman radiation.

So far, we discussed atomic processes related to atomic hydrogen. However, molecular hydrogen, having rich internal structure due to the presence of the rovibrational quantum states, can play an important role in high-density, low-temperature edge plasma phenomena. At low, ~few eV, electron temperatures, plasma cooling due to excitation of electronic states of neutrals and ions becomes less efficient because of the reduction of corresponding rate constants. At the same time, the cross-section of electron impact excitation of the vibrational states of molecular hydrogen, which goes through the metastable ion $H_2^{(-)}$ having relatively a low energy threshold [12], [17], [18], still remains large (see Fig.II.7). As a result, the effective "cooling" rate constant, $\tilde{K}_{cool} = \Delta E K_{\Delta E}$, (where ΔE is the electron energy loss due to excitation to some

quantum state and $K_{\Delta E}$ is the corresponding rate constant) for the excitation of the first vibrational level of H_2, $\tilde{K}_{cool}^{vibr}$, at small, ~1 eV, electron temperatures exceeds the cooling rate constant for the excitation of quantum state n=2 for atomic hydrogen, $\tilde{K}_{cool}^{1\to 2}$, (see Fig. II.8).

The vibrational states of a Hydrogen molecule in the background electronic state are virtually stable. Therefore, their incorporation into the CRM model (e.g. see [31]), which assumes that the population of all excited states is settled (due to spontaneous decay) on the time scale much shorter than the transport time scale, cannot be justified. As a result, the population of the vibrational states should be described with dynamic equations accounting for both molecular transport and electron impact excitation/deexcitation.

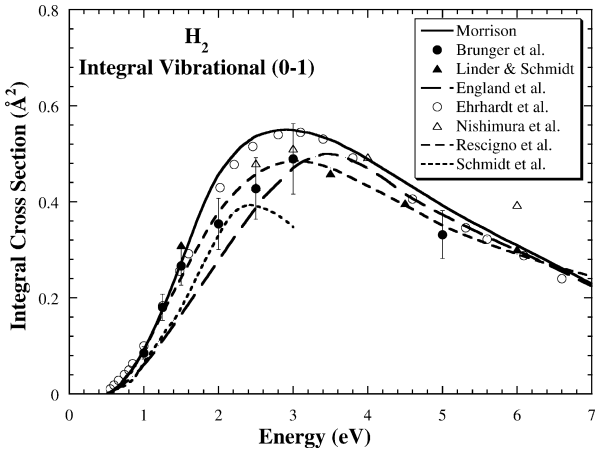

Fig. II.7. Experimental cross-section for the electron impact vibrational excitation of molecular hydrogen. Reproduced with permission from [61], © Elsevier 2002.

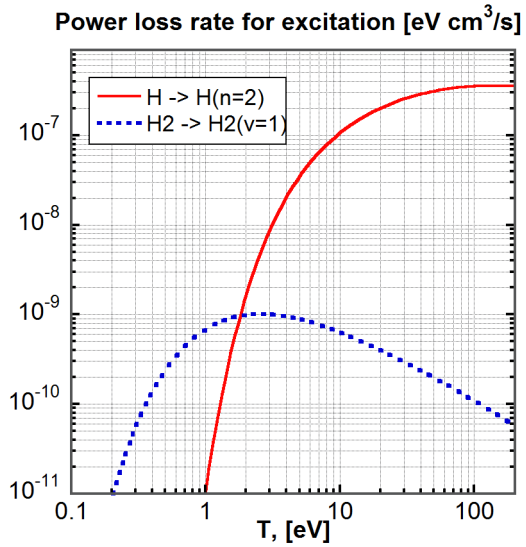

Fig. II.8. Cooling rate constants for the excitation of the first vibrational level of H_2 and quantum state n=2 for atomic hydrogen as functions of T_e.

The cross-sections of vibrational excitation $v \to v'$ by electron impact, $\sigma_{v\to v'}$, decreases with the increasing difference $|v - v'|$ [12] [62], [63] so that in practice, the main contribution to the population of the vibrational states of H_2 by electron impact is from excitation to the neighboring vibrational state $v \to v \pm 1$. In low temperature, weakly ionized plasma, an important role in the vibrational kinetics play the so-called vibrational-vibrational (V-V) exchange ($H_2(v) + H_2(v') \to H_2(v+1) + H_2(v'-1)$) and vibrational-translational (V-T) relaxation ($H_2(v) + M \to H_2(v' < v) + M$) processes where M is some atom/molecule (e.g. see [12], [64] and the references therein). Since the Massey parameter (e.g. see [12]) for the vibrational de-excitation caused by collisions with neutrals in low-temperature plasmas is large, the V-T relaxation is usually slow and the V-V exchange dominates. In this case, the distribution of molecules over vibrational states tends towards the Treanor function [65], which is

characterized by an overpopulation of highly excited states in comparison to the Boltzmann distribution. However, electron impact dissociation of $H_2(v)$, which increases with increasing v, along with other chemical reactions involving vibrationally excited molecules, occurring in edge plasmas, deplete the population of excited vibrational states with relatively high v.

Among the chemical reactions involving vibrationally excited molecules in the edge plasmas, the most important for our further consideration are the dissociative attachment (DA):

$$H_2(v) + e \rightarrow H^- + H, \qquad \text{(II.27)}$$

and ion conversion (IC):

$$H_2(v) + H^+ \rightarrow H_2^+ + H. \qquad \text{(II.28)}$$

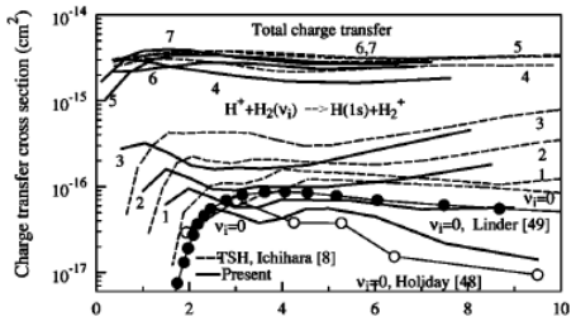

Fig. II.9. The dependence of the IC cross-section on the center of mass energy of colliding particles (in eV) for different vibrational quantum numbers (labeled with numbers in the figure) of H_2. Reproduced with permission from [59], © American Physical Society 1999.

Both of these processes are endothermic and, therefore, the cross-sections and the rate constants of both of these processes are very sensitive to the molecule vibrational excitation [66], [59]. In particular, the IC cross-section with the vibrational excitation above some threshold $v \geq v_{th} \propto \tilde{M}^{1/2}$, $v_{th} = 4$ for H_2, is by order of magnitude higher than that for $v = 3$, which is below the threshold (see Fig. II.9). Whereas DA plays a crucial role in the generation of intense, high, ~ 1 MeV, energy hydrogen neutral beams suitable for plasma heating in magnetic fusion reactors (e.g. see [64], [67] and the references therein), the IC following by the dissociative recombination (DR)

$$H_2^+ + e \rightarrow H + H,$$

turns out to be a significant plasma recombination sink in high density, low temperature, H divertor plasmas. However, in D (and T) divertor plasma, effective recombination through the DA channel followed by mutual neutralization of negative and positive hydrogen ions,

$$H^- + H^+ \rightarrow H + H, \qquad \text{(II.30)}$$

becomes more important [68]

We note that the products of the reactions (II.29) and (II.30) are in excited quantum states (from n=2 to n=4) and their further fate can be described by proper modification of the CRM.

The sequence of reactions (II.27)–(II.30) is known in magnetic fusion community as the Molecular Assisted Recombination (MAR) (e.g. see [69], [28], [70], [71], [68]).

Original estimates for the MAR rate [69], [28] performed for H_2 molecules demonstrated that MAR can be significantly faster than the EIR channel (see Fig. II.5) at temperatures ~few eV, where the EIR rate constant is small, and contribute significantly to the overall plasma recombination rate. However, unlike the EIR rate, which is not sensitive to the particular hydrogen isotope, the MAR rate is. This is because i) the vibrational excitation cross-section of a hydrogen molecule by electron impact decreases with an increase of the reduced mass $\tilde{M}$, $\sigma_{v \rightarrow v'}(\tilde{M}) \propto \tilde{M}^{-|v-v'|/2}$ [62]; and ii) the vibrational level corresponding to endothermic reactions

(II.27), (II.28) $v_{th} \propto \tilde{M}^{1/2}$ is increasing with the increase of $\tilde{M}$. Therefore, heavy isotopologues of a hydrogen molecule should encounter more interactions with electrons to reach v_{th}. As a result, one could expect a weaker effect of MAR for the case of tritium and deuterium plasmas in comparison with the hydrogen one. However, we notice that the overall contribution of MAR to plasma recombination depends on both spatial distribution of the plasma parameters and transport of molecules in low-temperature divertors and, therefore, is machine sensitive. The current version of MAR built into neutral the transport code EIRENE, which is used, in particular, for the simulations of edge plasma in ITER, assumes the CRM for the population of the vibrational states of hydrogen molecules (e.g. see [68] and the references therein).

In fusion-related experiments, the MAR effects were identified in the experiments on Alcator C-Mod [48] and linear divertor simulators [72], [73], [74]. Recent experimental data from TCV tokamak show that in detached divertor regime MAR can account for up to 40% of the overall plasma recombination sink [75].

II.4.2 Impurities

The energy loss due to impurity radiation plays an important role in many phenomena observed in the edge plasma, e.g. MARFE (which stands for the Multifaceted Asymmetric Radiation From the Edge) and divertor plasma detachment (see Chapter IX). Therefore, the data obtained with the CRM discussed above are widely used in both simplified estimates and comprehensive numerical simulations. Due to the relatively low density of impurity in the edge plasma in the "standard" regime of operation, trapping of impurity line radiation is not important. However, in some particular cases, where the generation of a dense cloud of impurities takes place (e.g. disruptions, injection of large dust grains into edge plasma, etc.), trapping of impurity line radiation becomes important (e.g. see [76], [77]).

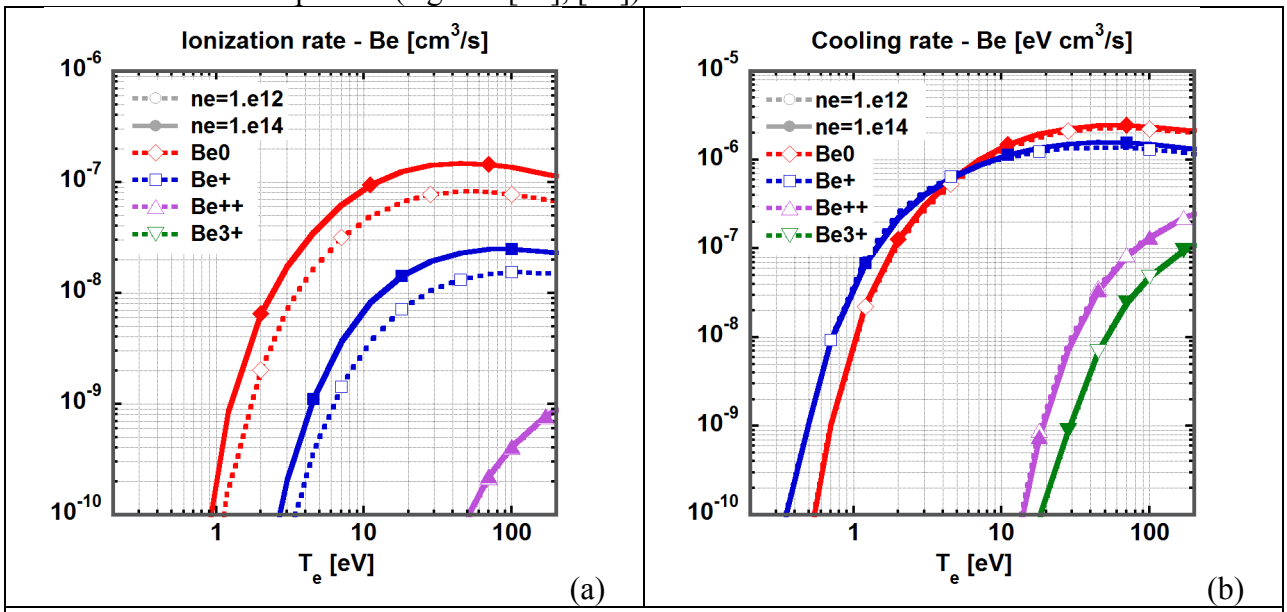

Fig. II.10. Dependence of the ionization (a) and cooling rate (b) constants for Be atom and first few Be ions on electron temperature for two different electron densities $n_e = 10^{12}\,\mathrm{cm}^{-3}$ and $n_e = 10^{14}\,\mathrm{cm}^{-3}$, obtained from the ADAS database.

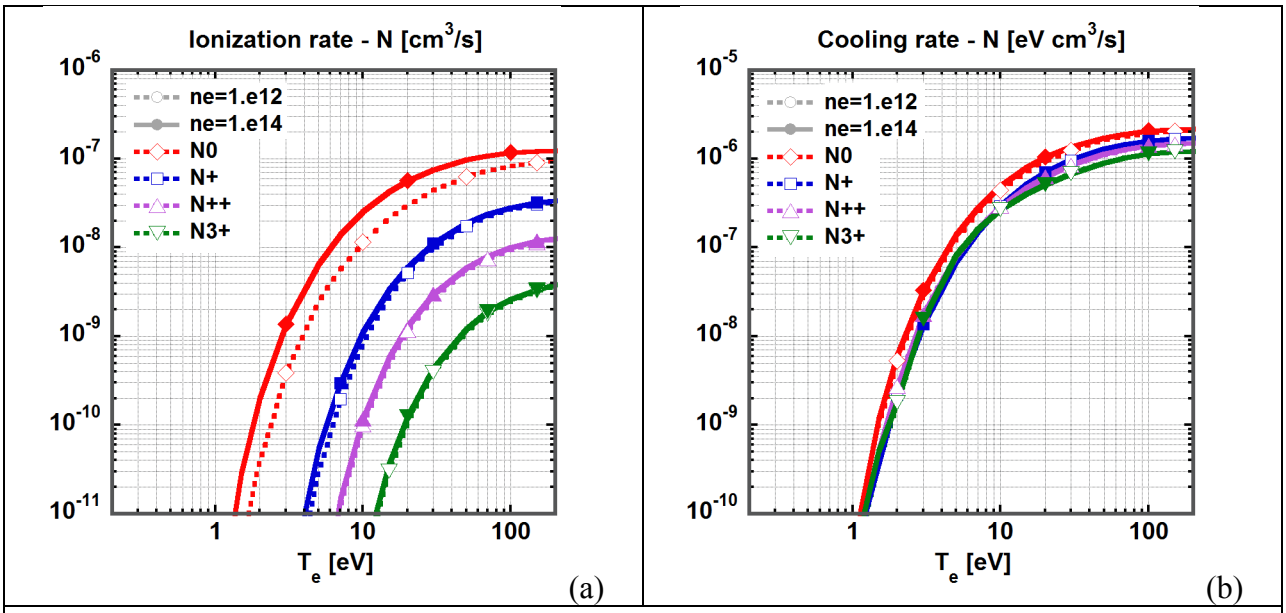

Fig. II.11. Dependence of the ionization (a) and cooling rate (b) constants for N atom and first few N ions on electron temperature for two different electron densities $n_e = 10^{12}\,\mathrm{cm}^{-3}$ and $n_e = 10^{14}\,\mathrm{cm}^{-3}$, obtained from the ADAS database.

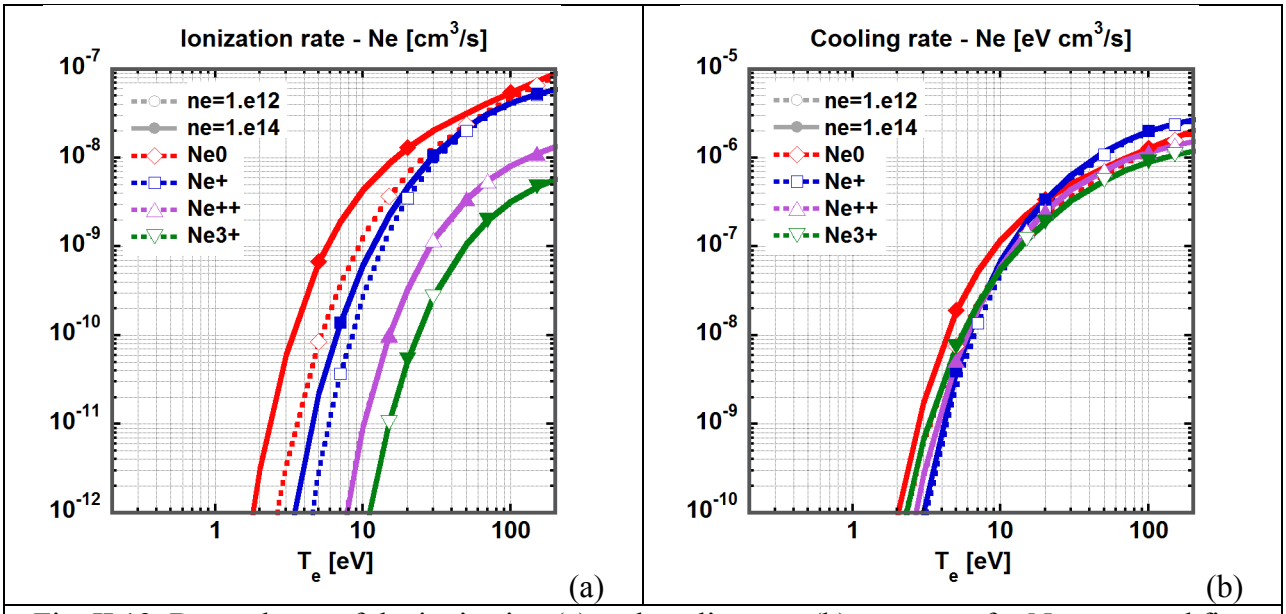

Fig. II.12. Dependence of the ionization (a) and cooling rate (b) constants for Ne atom and first few Ne ions on electron temperature for two different electron densities $n_e = 10^{12}\,\mathrm{cm}^{-3}$ and $n_e = 10^{14}\,\mathrm{cm}^{-3}$, obtained from the ADAS database.

Today, the main source of fusion-relevant atomic data including impurity, which is widely used in magnetic and astrophysical communities for both diagnostic purposes and numerical simulations, is the ADAS database [41], [30], which provides the rate constants for

different atomic processes, radiation energy loss by different charge states of many impurities, the contribution to the radiation loss of different lines, etc.

In this sub-section, we present particular examples of impurity charge state distribution and corresponding radiation energy loss and discuss some simplified models for the impurity radiation loss used in the literature.

In Figs. II.10-II.13 we show the dependence of the ionization and cooling rate constants for Be, N, Ne, and Ar on electron temperature for different electron densities, obtained from the ADAS database. These figures include neutrals and few first ionization states of corresponding impurities. As one can see from Figs.(II.10)-(II.13), the dependence of the ionization rate constant for impurity ions on electron density is not as strong as for atomic hydrogen (recall Fig. II.5), which indicates a weaker impact of the excited states of impurity ions due to the lower values of relevant spontaneous decay-time [30].

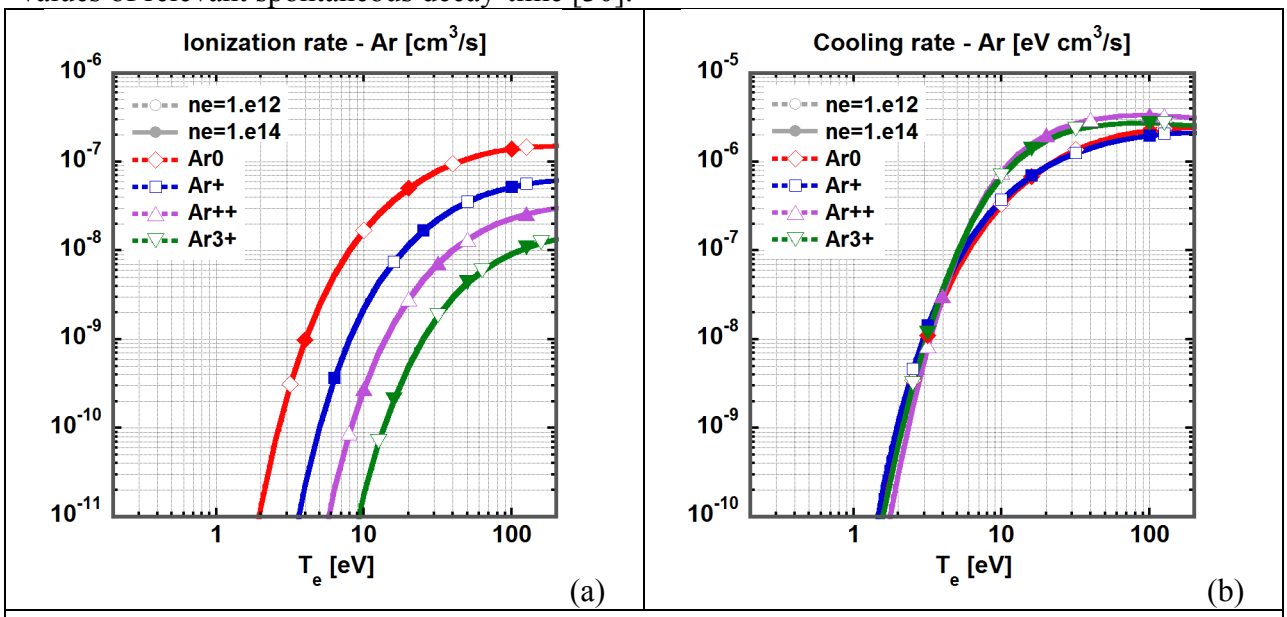

Fig. II.13. Dependence of the ionization (a) and cooling rate (b) constants for Ar atom and first few Ar ions on electron temperature, obtained from the ADAS database.

Such ionization, cooling, and recombination (not shown here) rate constants for impurities along with impurity transport models are used in edge plasma codes to assess an impact of impurity on plasma energy dissipation. However, these codes are very complex and to make an approximate evaluation of impurity radiation loss, some more tractable models are often used.

Recalling the CRM (e.g. for atomic hydrogen described by Eq. (II.12)-(II.13)), we find that the major simplification of the description of the population of excited states comes from the fact that the characteristic time for establishing the quasi-stationary population of excited states is shorter than the characteristic transport time. In this case, the population of excited states can be expressed in terms of the local density of atomic hydrogen Eq. (II.13), assuming that the nonlocal effects of radiation transport are not important. The same approximation is built into the description of excited states for every ionization state of impurity, but not for the distribution of the impurity ions over ionization states. The reason for this is that the characteristic equilibration time scale of the distribution of impurity over ionization states, τ_{imp}^{Z}, could be comparable with

or even longer than the characteristic impurity transport time scale, τ_{imp}^{transp}. If we assume that τ_{imp}^{transp} does not depend on the impurity charge state, we can write the following approximate balance equation for the impurity density in the Z-th ionization state n_Z ($Z>1$) for stationary plasma parameters [78]:

$$\frac{1}{n_e}\frac{d\xi_Z}{dt} = -\left(K_{ion}^Z + K_{rec}^Z\right)\xi_Z + K_{ion}^{Z-1}\xi_{Z-1} + K_{rec}^{Z+1}\xi_{Z+1} - \xi_Z\left(n_e\tau_{imp}^{transp}\right)^{-1} = 0, \qquad (II.31)$$

where K_{ion}^Z and K_{rec}^Z are the corresponding ionization and recombination rate constants, whereas $\xi_Z = n_Z / n_{imp}$ and $n_{imp} = \sum_Z n_Z$ are the partition of impurity density over ionization states and the total impurity density. Naturally, $K_{ion}^Z = 0$ for the highest charge state and $K_{rec}^Z = 0$ for the neutrals. In order to sustain the total impurity density, the transport term in Eq. (II.31) for neutrals ($Z=0$) is replaced with the corresponding source term. Note that writing ionization balance for the impurity ions this way, we imply that the transport processes simply remove the charged particles, replacing them by neutrals. Although in practice impurity transport is much more complex, such an approach gives a simple and useful estimate for the impurity radiation loss. By solving the algebraic equations (II.31) and neglecting three-body recombination of the impurity ions (which is only important at low temperatures where the impurity radiation loss is insignificant) we find that ξ_Z only depends on n_e, T_e, and $n_e\tau_{imp}^{transp}$. As a result, we can write the following expression for the volumetric plasma energy loss due to impurity radiation, W_{imp}^{rad}:

$$W_{imp}^{rad} = n_e n_{imp}\sum_Z \tilde{K}_{cool}^Z \xi_Z\left(n_e, T_e, n_e\tau_{imp}^{transp}\right) \equiv n_e n_{imp}\tilde{L}_{imp}\left(n_e, T_e, n_e\tau_{imp}^{transp}\right). \qquad (II.32)$$

Taking $\tau_{imp}^{transp} \to \infty$ and neglecting dependence of $\tilde{L}_{imp}$ on electron density, we come to the so-called "coronal approximation" for the impurity radiation loss, $\tilde{L}_{imp} \equiv L_{imp}(T_e)$, which is often used in analytic and semi-analytic models. The function $L_{imp}(T_e)$ is shown in Fig. II.14 for most common impurities in fusion plasmas.

The finite τ_{imp}^{transp} implies the volumetric source of impurity, $S_{imp} = n_{imp} / \tau_{imp}^{transp}$. By combining W_{imp}^{rad} and S_{imp}, it is useful to introduce an effective neutral impurity "ionization cost", E_{ion}^{imp}:

$$E_{ion}^{imp} = W_{imp}^{rad} / S_{imp} = n_e\tau_{imp}^{transp}\tilde{L}_{imp}\left(n_e, T_e, n_e\tau_{imp}^{transp}\right), \qquad (II.33)$$

which is just an analog of the hydrogen ionization cost.

In Fig. II.15 one can find the dependencies of W_{imp}^{rad} (a) and E_{ion}^{imp} (b) for N on electron temperature for the electron density $n_e = 10^{14}\,cm^{-3}$ and different values of $n_e\tau_{imp}^{transp}$ calculated with the ADAS database. Similar dependencies, but for Ne, are shown in Fig. II.16. As one can see from Figs. (II.15) and (II.16), in both cases $E_{ion}^{imp} \sim$ few keV if the impurity ion confinement is good ($n_e\tau_{imp}^{transp} \sim 10^{10}\,s\cdot cm^{-3}$). The estimate $E_{ion}^{imp} \sim$ few keV is consistent with the experimental and simulation results from Refs. [80], [81], where the so-called impurity "radiation potential" (having the physical meaning somewhat similar to E_{ion}^{imp}) was introduced.

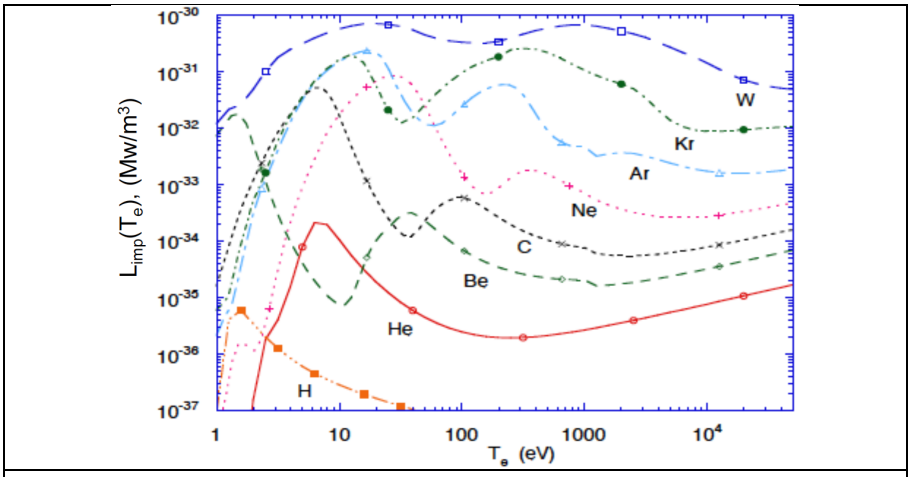

Fig. II.14. Cooling rates $L_{imp}(T_e)$ for different impurities calculated in "coronal approximation". Reproduced with permission from [79], © IAEA 1999.

According to [80], the "radiation potential" for carbon is about 3 keV at $T_e \sim 20$ eV and falls to ~ 1 keV at $T_e \sim 60$ eV, showing the trend consistent with Fig. II.15. Comparing $E_{ion}^{imp} \sim$ few keV and $E_{ion}^{H} \sim 30$ eV, we can conclude that impurity starts to dominate the energy loss from edge plasma when the impurity fraction in the total flux of neutrals into the plasma from the PFCs exceeds ~1%.

The equations (II.31) can be extended by incorporation of charge-exchange between the impurity ion and hydrogen atom $A^{z+1} + H \rightarrow A^{Z}(n) + H^{+}$ (e.g. see [82]), which introduces in the function $\tilde{L}_{imp}$ one more free parameter, the ratio $[H]/n_e$. This effect could also increase the impurity radiation loss at high electron temperatures [82], [20]. However, neutral hydrogen is not abundant at high temperatures.

Conclusions for Ch. II

In conclusion to this chapter, it would be fair to say that our knowledge of atomic processes in the edge plasma is reasonable with respect to both understanding of the main physical processes and completeness of the data needed to model and diagnose the most critical processes in the edge plasma of fusion devices. It is not surprising because our studies in this area are based on the century-old effort of a few generations of scientists. Nonetheless, some additional data would be needed for the case where the transport processes in edge plasma should be described kinetically. However, incorporation of plasma kinetic processes and radiation transport effects into edge plasma modeling tools is beyond current computer capabilities. We notice also that the addition of the radiation-induced transitions between different quantum states (e.g. for hydrogen

atoms) for opaque regimes, relevant for detached divertor plasmas in fusion reactors such as ITER, make the simulations of the edge plasma parameters very "expensive" computationally. Therefore, there are only a few cases where such effects were accounted for.

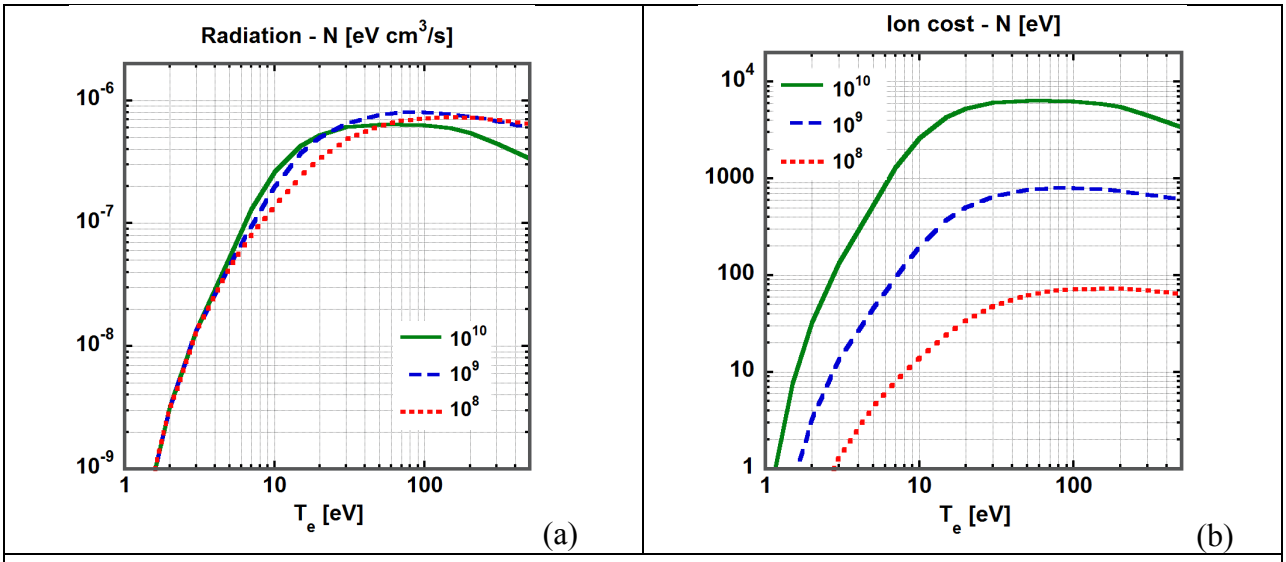

Fig. II.15. Dependence of W_{imp}^{rad} (a) and E_{ion}^{imp} (b) for N on electron temperature for the electron density $n_e = 10^{14}\,cm^{-3}$ and different values of $n_e\tau_{imp}^{transp}$ for 10^{10}, 10^9, and 10^8 s cm^{-3}, calculated with the ADAS database.

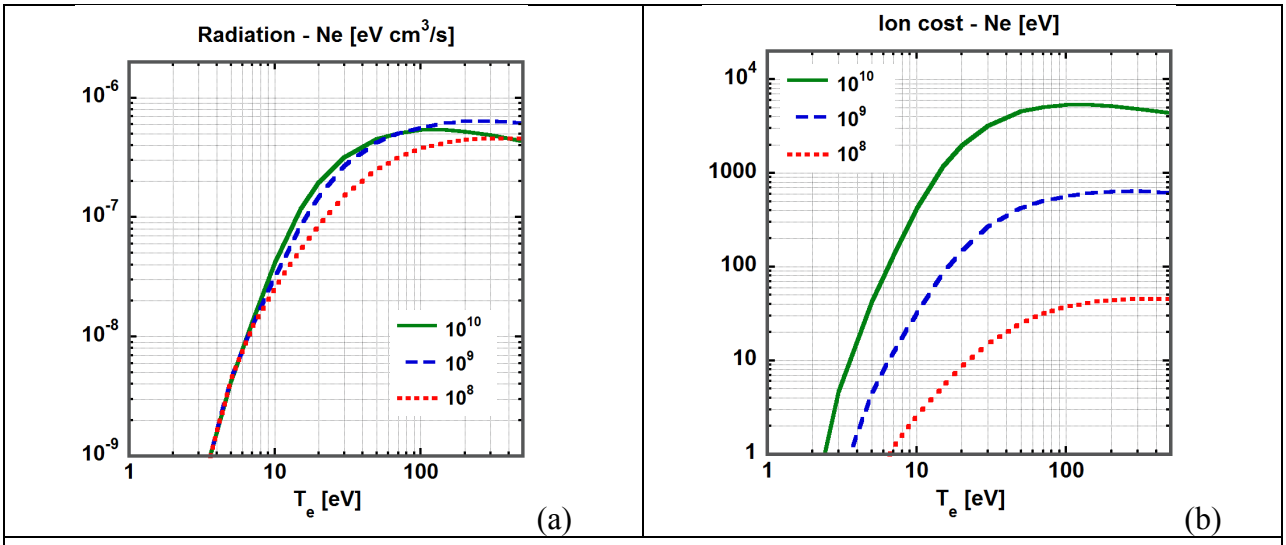

Fig. II.16. Dependence of W_{imp}^{rad} (a) and E_{ion}^{imp} (b) for Ne on electron temperature for the electron density $n_e = 10^{14}\,cm^{-3}$ and different values of $n_e\tau_{imp}^{transp}$ for 10^{10}, 10^9, and 10^8 s cm^{-3}, calculated with the ADAS database.

References for Chapter II

[1] Yu. P. Raizer "Gas Discharge Physics", Springer, 1991

[2] M. A. Lieberman and A. J. Lichtenberg "Principals of Plasma Discharges and Material Processing", John Wiley & Sons, Inc., NY 2005

[3] B. M. Smirnov "Physics of Ionized Gases", John Wiley & Sons, Inc., NY 2007

[4] L. D. Landau and L. M. Lifshitz "Quantum Mechanics (Non-Relativistic Theory)", Course of Theoretical Physics, Volume 3, Third Edition, Elsevier Ltd. 2005.

[5] Ya. B. Zeldovich, G. I. Barenblatt, V. B. Librovich, G. M. Makhviladze, "The mathematical theory of combustion and explosions", Kluiver Academic Publisher Group, Dordrecht, Netherland, 1985.

[6] F. A. Williams "Combustion theory", Second Edition, The Benjamin/Cummings Publishing Company, Inc., 1985.

[7] D. R. Inglis and E. Teller, "Ionic Depression of Series Limits in One-Electron Spectra" Astrophys. J. **90** (1939) 439-442.

[8] L. G. D'yachkov "Smooth Transition from Spectral Lines to a Continuum in Dense Hydrogen Plasma", High Temperature **54** (2016) 3-10.

[9] K. Tsumori, K. Ikeda, H. Nakano, M. Kisaki, S. Geng, M. Wada, K. Sasaki, S. Nishiyama, M. Goto, G. Serianni, P. Agostinetti, E. Sartori, M. Brombin, P. Veltri, C. Wimmer, K. Nagaoka, M. Osakabe, Y. Takeiri, and O. Kaneko, "Negative ion production and beam extraction processes in a large ion source", Rev. Scientific Instr. **87** (2016) 02B936.

[10] S. S. Hodgman, R. G. Dall, L. J. Byron, K. G. H. Baldwin, S. J. Buckman, and A. G. Truscott, "Metastable Helium: A New Determination of the Longest Atomic Excited-State Lifetime", Phys. Rev. Lett. **103** (2009) 053002.

[11] R. S. Van Dyck, Jr., C. E. Johnson, and H. A. Shugart, "Radiative Lifetime of the 2^1S_0 Metastable State of Helium", Phys. Rev. A, General Phys. **4** (1971) 1327-1336.

[12] L. M. Biberman, V. S. Vorob'ev, and I. T. Yakovlev, "Kinetics of Nonequilibrium Low-Temperature Plasma", Consultants Bureau, New York, 1987

[13] T. Fujimoto, "A collisional-radiative model for helium and its application to a discharge plasma", J. Quant. Spectrosc. Radiat. Transfer **21** (1979) 439-455

[14] P. E. Siska "Molecular-beam studies of Penning ionization", Rev. Mod. Phys. **65** (1993) 337-412.

[15] R. E. Moss and I. A. Sadler, "Symmetry breaking effects in HD^+", Mol. Phys. **61** (1989) 905-921.

[16] M. Capitelli, G. Colonna, A. D'Angola, "Fundamental Aspects of Plasma Chemical Physics: Thermodynamics", Springer Series on Atomic, Optical, and Plasma Physics **66**, Springer Science+Business Media, LLC 2012, Appendix A, p. 293.

[17] F. R. Gilmore, E. Bauer, and J. W. McCowan, "A review of atomic and molecular excitation mechanisms in nonequilibrium gases up to 20,000 K", J. Quant. Spectrosc. Radiat. Transfer **9** (1969) 157-183.

[18] J. N. Bardsley and J. M. Wadehra, "Dissociative attachment and vibrational excitation in low-energy collisions of electrons with H_2 and D_2", Phys. Rev. A **20** (1979) 1398-1405.

[19] R. K. Janev, W. D. Langer, K. Evans, D. E. Post, "Elementary Processes in Hydrogen–Helium Plasmas", Springer, Berlin (1987).

[20] D. E. Post, "A review of recent developments in atomic processes for divertors and edge plasmas", J. Nucl. Materials **220–222** (1995) 143-157.

[21] R. K. Janev, (Ed.), Atomic and Molecular Processes in Fusion Edge Plasmas, Plenum, New York, NY (1995).
[22] L. D. Landau and L. M. Lifshitz "Physical Kinetics", Course of Theoretical Physics, Volume 10, Elsevier Ltd. 2010.
[23] M. Capitelli, R. Celiberto, G. Colonna, F. Esposito, C. Gorse, K. Hassouni, A. Laricchiuta, S. Longo, "Fundamental Aspects of Plasma Chemical Physics, Kinetics", Springer Series on Atomic, Optical, and Plasma Physics **85**, Springer, New York 2016, pp. 143-173.
[24] V. I. Fisher, Yu. V. Ralchenko, V. A. Bernshtam, A. Goldgirsh, Y. Maron, L. A. Vainshtein, I. Bray, H. Golten, "Electron-impact-excitation cross sections of hydrogenlike ions", Phys. Rev. A **55** (1997) 329-334.
[25] D. R. Bates, A. E. Kingston and R. W. P. McWhirter, "Recombination between electrons and atomic ions I. Optically this plasmas", Proc. R. Soc. A **267** (1962) 297-312.
[26] D. R. Bates, A. E. Kingston and R. W. P. McWhirter, "Recombination between electrons and atomic ions II. Optically thick plasmas", Proc. R. Soc. A **270** (1962) 155-167.
[27] K. Sawada, Y. Yamada, T. Miyachika, N. Ezumi, A. Iwamae, and M. Goto, "Collisional-Radiative Model for Spectroscopic Diagnostic of Optically Thick Helium Plasma", Plasma Fus. Res. **5** (2010) 001.
[28] A. Yu. Pigarov, S. I. Krasheninnikov, "Application of the collisional-radiative, atomic-molecular model to the recombining divertor plasma" Phys. Lett. A **222** (1996) 251-257.
[29] B. van der Sijde, J. J. A. M. van der Mullen and D. C. Schram. "Collisional Radiative Models in Plasmas" Beitr. Plasmaphys. **24** (1984) 447-473
[30] H. P. Summers, W. J. Dickson, M. G. O'Mullane, N. R. Badnell, A. D. Whiteford, D. H. Brooks, J. Lang, S. D. Loch, and D. C. Griffin, "Ionization state, excited populations and emission of impurities in dynamic finite density plasmas: I. The generalized collisional–radiative model for light elements" Plasma Phys. Contr. Fusion **48** (2006) 263-293.
[31] K. Sawada and M. Goto "Rovibrationally Resolved Time-Dependent Collisional-Radiative Model of Molecular Hydrogen and Its Application to a Fusion Detached Plasma", Atoms **4** (2016) 29.
[32] R. K. Janev, C. J. Joachain, N. N. Nedeljković, "Resonant electron transfer in slow collisions of protons with Rydberg hydrogen atoms", Phys. Rev. A **29** (1984) 2436-2469.
[33] S. I. Krasheninnikov and A. S. Kukushkin "Physics of ultimate detachment of a tokamak divertor plasma" J. Plasma Phys. **83** (2017) 155830501.
[34] V. A. Abramov, V. S. Lisitsa, and A, Yu. Pigarov, "Changes in effective charge-exchange cross-sections in a plasma" JTP Lett. **42** (1985) 356-359.
[35] P. Helander, S. I. Krasheninnikov, and P. J. Catto, "Fluid equations for a partially ionized plasma", Phys. Plasmas **1** (1994) 3174-3180.
[36] S. I. Krasheninnikov, A. Yu. Pigarov, "Kinetics of atoms in multistep excitation processes in plasma", Contr. Plasma Phys. **28** (1988) 345-346.
[37] S. I. Krasheninnikov, V. S. Lisitsa, A. Yu. Pigarov, "Charge exchange in a divertor plasma with excited particles", Sov. J. Plasma Phys. **14** (1988) 612-616.
[38] V. P. Zhdanov, "Dielectronic recombination", in Review of Plasma Physics, edited by M. A. Leontovich and B. B. Kadomtsev, Consultants Bureau, New York, 1987, vol. 12, p. 103
[39] Y. Hahn, "Electron-Ions Recombination processes in Plasmas", in Janev, R.K. (Ed.), Atomic and Molecular Processes in Fusion Edge Plasmas, Plenum, New York, NY (1995), p.91

[40] V. S. Lisitsa, M. B. Kadomtsev, V. Kotov, V. S. Neverov, and V. A. Shurygin, "Hydrogen Spectral Line Shape Formation in the SOL of Fusion Reactor Plasmas", Atoms **2** (2014) 195-206.
[41] See website http://open.adas.ac.uk/
[42] D. Reiter, "The EIRENE Code User Manual," *http://www.eirene.de*. 2017.
[43] S. I. Krasheninnikov, A. Yu. Pigarov, "Superhigh density operating conditions for a poloidal divertor in a tokamak reactor", Nuclear Fusion Suppl. **3** (1987) 387-394.
[44] R. Marchand, and J. Lauzon, "Hydrogen recycling with multistep and resonance line absorption effects" Phys. Fluids **4** (1992) 924-933.
[45] D. Reiter, V. Kotov, P. Börner, K. Sawada, R. K. Janev, B. Küpers, "Detailed atomic, molecular and radiation kinetics in current 2D and 3D edge plasma fluid codes", Journal of Nuclear Materials **363-365** (2007) 649-657.
[46] T. Fujimoto, "Plasma Spectroscopy"; The International Series of Monographs on Physics, **123**; Oxford University Press; Oxford, UK, 2004.
[47] V. I. Kogan, V. S. Lisitsa, G. V. Sholin, "Spectral line broadening in plasma", in Review of Plasma Physics, edited by B. B. Kadomtsev, Consultants Bureau, New York, 1987, vol. 13, p. 261.
[48] J. L.Terry, B. Lipschultz, A. Yu. Pigarov, S. I. Krasheninnikov, B. LaBombard, D. Lumma, H. Ohkawa, D. Pappas, & M. Umansky, "Volume recombination and opacity in Alcator C-Mod divertor plasmas". *Phys. Plasmas* **5**, (1998) 1759-1766.
[49] H. R. Griem, "Principals of Plasma Spectroscopy", Cambridge University Press, 1997.
[50] V. A. Abramov, V. I. Kogan, and V. S. Lisitsa, "Radiative Transfer in Plasma" in Review of Plasma Physics, edited by M. A. Leontovich and B. B. Kadomtsev, Consultants Bureau, New York, 1987, vol. 12, p. 151.
[51] M. L. Adams, H. A. Scott, R. W. Lee, J. L. Terry, E. S. Marmar, B. Lipschultz, A. Yu. Pigarov, J. P. Freidberg, "Application of magnetically-broadened hydrogenic line profiles to computational modeling of a plasma experiment", J. Quant. Spectr. Rad. Transfer **71** (2001) 117-128.
[52] D. Reiter, M. Baelmans, and P. Börner, "The EIRENE and B2-EIRENE Codes", Fus. Science Techn. **47** (2005) 172-186.
[53] V. Kotov, D. Reiter, A. S. Kukushkin, H. D. Pacher, P. Bőrner, and S. Wiesen, "Radiation absorption effects in B2-EIRENE divertor modelling", Contr. Plasma Phys. **46** (2006) 635-642.
[54] H. A. Scott, "Cretin-a radiative transfer capability for laboratory plasmas", J. Quant. Spectr. Rad. Transfer **71** (2001) 689.
[55] H. A. Scott, M. L. Adams, "Incorporating Line Radiation Effects into Edge Plasma Codes", Contrib. Plasma Phys, **44** (2004) 51-56.
[56] M. L. Adams, H. A. Scott, "Effect of hydrogen line radiation on the divertor target plate incident heat flux", Contrib. Plasma Phys, **44** (2004) 262-267.
[57] V. Kotov and D. Reiter, "Formation of a natural X-point multifaceted asymmetric radiation from the edge in numerical simulations of divertor plasmas", Plasma Phys. Control. Fusion **54** (2012) 082003.
[58] P. S. Krstic and D. R. Schultz, "Elastic scattering and charge transfer in slow collisions: isotopes of H and H^+ colliding with isotopes of H and with He", J. Phys. B: At. Mol. Opt. Phys. **32** (1999) 3485-3509.

[59] P. S. Krstic, "Inelastic processes from vibrationally excited states in slow H^++H_2 and H+H_2 collisions: Excitations and charge transfer", Phys. Rev. A **66** (2002) 042717.
[60] R. K. Janev, D. E. Post, W. D. Langer, K. Evans, D. B. Heifetz And J. C. Weisheit, "Survey of atomic processes in edge plasmas", J. Nucl. Mater. **121** (1984) 10-16.
[61] M. J. Brunger, S. J. Buckman, "Electron–molecule scattering cross-sections . I . Experimental techniques and data for diatomic molecules", Physics Reports **357** (2002) 215-458.
[62] D. E. Atems and J. M. Wadehra, "Vibrational excitation of H_2 and HCl by low-energy electron impact. An isotope scaling law", Chem. Phys. Lett. **197** (1992) 525-529.
[63] M. Capitelli, R. Celiberto, F. Esposito, A. Laricchiuta, K. Hassouni and S. Longo, "Elementary processes and kinetics of H_2 plasmas for different technological applications", Plasma Sources Sci. Technol. **11** (2002) A7–A25.
[64] F. Gaboriau and J. P. Boeuf, "Chemical kinetics of low pressure high density hydrogen plasmas: application to negative ion sources for ITER", Plasma Sources Sci. Technol. **23** (2014) 065032.
[65] C. E. Treanor, J. W. Rich, and R. G. Rehm, "Vibrational Relaxation of Anharmonic Oscillators with Exchange-Dominated Collisions", J. Chem. Phys. **48** (1968) 1798-1807.
[66] J. M. Wadehra, "Dissociative attachment to rovibrationally excited H_2", Phys. Rev. A **29** (1984) 106-110.
[67] M. Bacal and M. Wada, "Negative hydrogen ion production mechanisms", Appl. Phys. Rev. **2** (2015) 021305.
[68] A. S. Kukushkin, S. I. Krasheninnikov, A. A. Pshenov, D. Reiter, "Role of molecular effects in divertor plasma recombination", Nucl. Mater. Energy **12** (2017) 984-988.
[69] S. I. Krasheninnikov, A. Yu. Pigarov, D. J. Sigmar, "Plasma recombination and divertor detachment" Phys. Lett. A **214** (1996) 285-291.
[70] D. Reiter, Chr. May, M. Baelmans, P. Börner, "Non-linear effects on neutral gas transport in divertors", J. Nucl. Mater. **241-243** (1997) 342-348.
[71] R. K. Janev, "Alternative Mechanisms for Divertor Plasma Recombination", Phys. Scripta **T96** (2002) 94-101.
[72] N. Ohno, N. Ezumi, S. Takamura, S. I. Krasheninnikov, & A. Yu. Pigarov, "Experimental evidence of molecular activated recombination in detached recombining plasmas", Phys. Rev. Lett. **81** (1998) 818–821.
[73] A. Tonegawa, M. Ono, Y. Morihira, H. Ogawa, T. Shibuya, K. Kawamura, K. Takayama, "Observation of molecular assisted recombination via negative ions formation in a divertor plasma simulator, TPDSHEET-IV", J. Nucl. Mater. **313-316** (2003) 1046-1051.
[74] A. Okamoto, S. Kado, K. Sawada, Y. Kuwahara, Y. Iida, S. Tanaka, "Contribution of hydrogen molecular assisted recombination processes to population of hydrogen atom in divertor simulator MAP-II" J. Nucl. Mater. **363-365** (2007) 395-399.
[75] B. Lipshchultz, private communication, 2019.
[76] V. Sizyuk and A. Hassanein, "Heat loads to divertor nearby components from secondary radiation evolved during plasma instabilities", Phys. Plasmas **22** (2015) 013301.
[77] A. A. Pshenov, A. S. Kukushkin, E. D. Marenkov, and S. I. Krasheninnikov, "On the role of hydrogen radiation absorption in divertor plasma detachment", Nucl. Fusion. **59** (2019) 106025.
[78] R. A. Hulse, "Numerical studies of impurities in fusion plasmas", Nucl. Techn.-Fusion **3** (1983) 259-272.

[79] ITER Physics Basis, Chapter 4: Power and particle control. Nucl. Fusion **39** (1999) 2391-2469.
[80] U. Samm, P. Bogen, H.A. Claassen, H. Gerhauser, H. Hartwig, E. Hintz, Y.T. Lie, A. Pospieszczyk, D. Rusbüldt, and B. Schweer, "Influence of impurity radiation losses on plasma edge properties in TEXTOR", J. Nucl. Mater. **176-177** (1990) 273-277.
[81] M. Z. Tokar and F. A. Kelly, "The role of plasma–wall interactions in thermal instabilities at the tokamak", Phys. Plasma **10** (2003) 4378-4386.
[82] S. L. Allen, M. E. Rensink, D. N. Hill, R. Wood, D. Nilson, B. G. Logan, R. Stambaugh, T. W. Petrie, G. M. Steabler, M. A. Mahdavi, R. Hulse, R. B. Campbell, "A design study for an advanced divertor for DIII-D and ITER: the radiative slot divertor", J. Nucl. Mater. **196-198** (1992) 804-809.